Article

Cell Systems

Multi-layer CRISPRa/i circuits for dynamic genetic programs in cell-free and bacterial systems

Graphical abstract

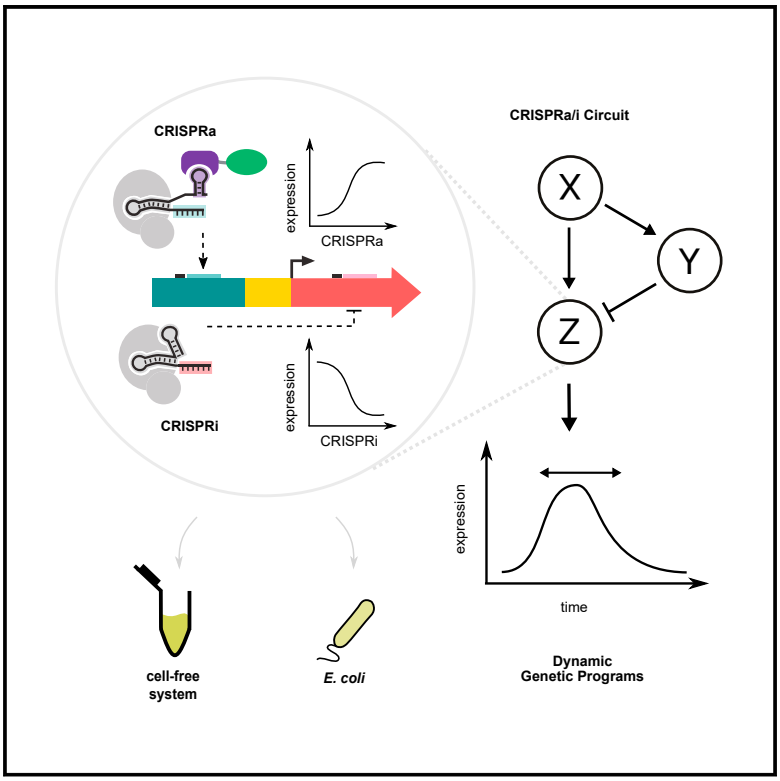

Authors

Benjamin I. Tickman,
Diego Alba Burbano,
Venkata P. Chavali, ...,
Vincent Noireaux, Jesse G. Zalatan,
James M. Carothers

Correspondence

zalatan@uw.edu (J.G.Z.),
jcaroth@uw.edu (J.M.C.)

In brief

Modular and tunable CRISPRa/i circuits provide a scalable paradigm for engineering dynamic gene regulatory networks.

Highlights

- Integration of CRISPRa with CRISPRi greatly expands genetic circuit design space
- Level-matching of multi-layer circuits is achieved via regulated expression of gRNAs
- Rational tuning of gRNA expression levels programs distinct gene expression dynamics
- Multi-guide circuit functions highlight the potential for scalable circuit design

Tickman et al., 2022, Cell Systems *13*, 215–229
March 16, 2022
https://doi.org/10.1016/j.cels.2021.10.008

CellPress

Cell Systems

CellPress

Article

Multi-layer CRISPRa/i circuits for dynamic genetic programs in cell-free and bacterial systems

Benjamin I. Tickman,[1,5] Diego Alba Burbano,[1,2,5] Venkata P. Chavali,[1] Cholpisit Kiattisewee,[1] Jason Fontana,[1] Aset Khakimzhan,[3] Vincent Noireaux,[3] Jesse G. Zalatan,[1,4,*] and James M. Carothers[1,2,6,*]

[1]Molecular Engineering & Sciences Institute and Center for Synthetic Biology, University of Washington, Seattle, WA 98195, USA
[2]Department of Chemical Engineering, University of Washington, Seattle, WA 98195, USA
[3]School of Physics and Astronomy, University of Minnesota, Minneapolis, MN 55455, USA
[4]Department of Chemistry, University of Washington, Seattle, WA 98195, USA
[5]These authors contributed equally
[6]Lead contact
*Correspondence: zalatan@uw.edu (J.G.Z.), jcaroth@uw.edu (J.M.C.)
https://doi.org/10.1016/j.cels.2021.10.008

SUMMARY

CRISPR-Cas transcriptional circuits hold great promise as platforms for engineering metabolic networks and information processing circuits. Historically, prokaryotic CRISPR control systems have been limited to CRISPRi. Creating approaches to integrate CRISPRa for transcriptional activation with existing CRISPRi-based systems would greatly expand CRISPR circuit design space. Here, we develop design principles for engineering prokaryotic CRISPRa/i genetic circuits with network topologies specified by guide RNAs. We demonstrate that multi-layer CRISPRa/i cascades and feedforward loops can operate through the regulated expression of guide RNAs in cell-free expression systems and *E. coli*. We show that CRISPRa/i circuits can program complex functions by designing type 1 incoherent feedforward loops acting as fold-change detectors and tunable pulse-generators. By investigating how component characteristics relate to network properties such as depth, width, and speed, this work establishes a framework for building scalable CRISPRa/i circuits as regulatory programs in cell-free expression systems and bacterial hosts.
A record of this paper's transparent peer review process is included in the supplemental information.

INTRODUCTION

Inspired by nature, synthetic biologists seek to dynamically regulate gene expression in biological systems to conserve resources, respond to stimuli, and generate complex, time-dependent behavior (Brockman and Prather, 2015; Dinh and Prather, 2020; Fontana et al., 2018a; Santos-Moreno and Schaerli, 2020). However, there are limited examples of synthetic, dynamic transcriptional regulatory networks capable of complex, multi-gene regulation. This rarity can be attributed to the limited number of suitable components for implementing scalable regulatory networks (English et al., 2021; Jeong et al., 2019; Nielsen et al., 2016), and to the difficulty of sequentially combining components into multi-layer operations (Brophy and Voigt, 2014; Gander et al., 2017; Lucks et al., 2008; Qian et al., 2017). Hence, a scalable framework enabling rational design and tuning of dynamic regulatory programs would constitute a significant advance.

CRISPR-Cas transcriptional controls have emerged as a promising route for building gene regulatory networks enabling programmable and orthogonal control at many loci simultaneously (Banerjee et al., 2020; Landberg et al., 2020; Reis et al., 2019; Tian et al., 2019). In these systems, nuclease-defective Cas proteins such as *S. pyogenes* dCas9 are combined with guide RNAs (gRNAs) that specify DNA targets. Targeting of this complex to promoters or open reading frames generates gene repression (CRISPRi). Scalable multi-gene circuits can thus be implemented simply through the programed expression of multiple gRNAs (Gander et al., 2017; Huang et al., 2021; Nielsen and Voigt, 2014; Santos-Moreno et al., 2020). Recent efforts have demonstrated the construction of CRISPRi circuits capable of performing a diverse set of Boolean logic evaluations (Gander et al., 2017; Nielsen and Voigt, 2014; Tan and Ng, 2021; Xiang et al., 2018), and dynamic expression programs (Dinh and Prather, 2019; Tian et al., 2020; Westbrook et al., 2019; Wu et al., 2020b). The recent discovery of new transcriptional activators and promoter design rules for effective CRISPR activation (CRISPRa) in bacteria raised the possibility of circuits combining CRISPRa and CRISPRi to form dynamic gene regulatory networks in prokaryotic systems (Dong et al., 2018; Fontana et al., 2020; Kiattisewee et al., 2021; Liu et al., 2019). Such circuits would enable network topologies and functional capabilities not possible with CRISPRi alone. Implementation of simultaneous CRISPRa and CRISPRi has been demonstrated on both multiple and individual genes (Table S2) (Dong et al., 2018; Kiattisewee et al., 2021; Wu et al., 2020a). In this

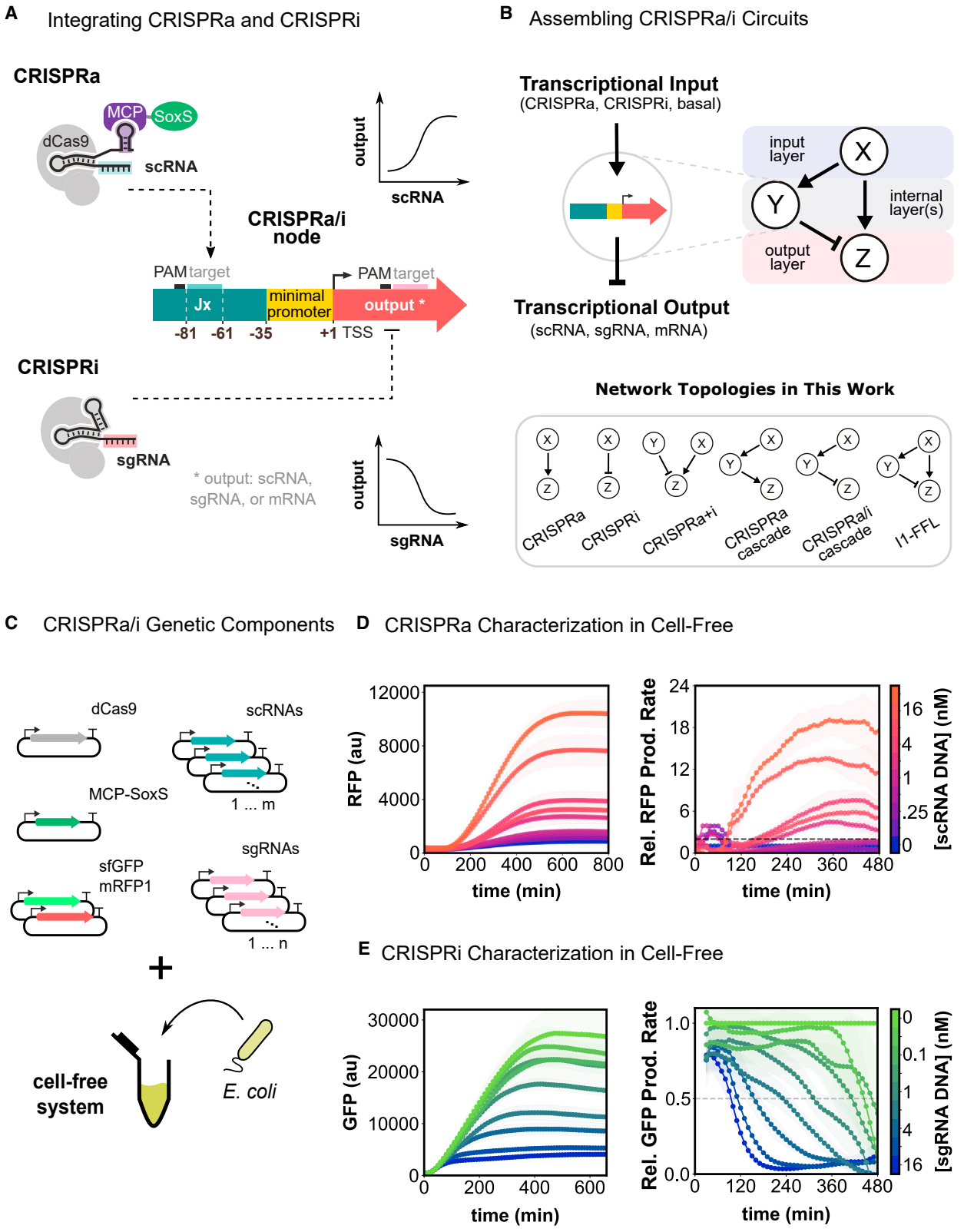

Figure 1. Combining CRISPRa with CRISPRi expands CRISPR circuit design space

(A) Schematic of CRISPRa/i nodes. Modified guide RNAs (scaffold RNAs or scRNAs) include a 3′ MS2 hairpin to recruit a transcriptional activator fused to the MS2 coat protein (MCP). The expression of scRNAs targeted to an appropriate site upstream of the promoter results in CRISPR transcriptional activation (CRISPRa)

(legend continued on next page)

work, we endeavored to apply CRISPRa in genetic circuits that go beyond elementary operations in a single layer (Bikard et al., 2013; English et al., 2021; Fontana et al., 2020; Liu et al., 2019; Ho et al., 2020; Liu et al., 2014).

Here, we develop genetic components and design strategies allowing CRISPRa to be combined with CRISPRi to generate a multi-layer CRISPRa/i transcriptional control system operating in *E. coli* and an *E. coli*-derived cell-free expression system (CFS). We show that the strength and dynamics of control actions can be tuned through the regulated expression of guide RNAs, with CRISPR activation ratios as high as 25-fold in CFS and 40-fold in *E. coli*. We combine components into multi-layered operations by level-matching the output expression levels of upstream components to the acceptable input range of downstream components (McDaniel and Weiss, 2005; Wang et al., 2013). We report the successful construction and tuning of multi-guide CRISPRa/i cascades and type 1 incoherent feed-forward loops (I1-FFLs) in CFS and *E. coli* to programmably achieve complex behaviors such as pulse generation and fold-change detection. Together, a set of generalizable design rules and an expandable toolbox of orthogonal components provide a framework for rapid and scalable implementation of higher order CRISPRa/i regulatory networks. We envision that these capabilities will prove useful for the next generation of dynamically regulated metabolic engineering efforts, multiplexed biosensing, and self-adaptive biocomputation (Bartoli et al., 2020; Wan et al., 2019; Wu et al., 2020b).

RESULTS

CRISPRa/i circuits in CFS

Bacterial CRISPRa is functional in E. coli *CFS*

Cell-free systems have become an attractive platform for prototyping of genetic circuits, construction of synthetic cells, and engineered biosynthetic pathways (Adamala et al., 2017; Dudley et al., 2015; Garamella et al., 2016; Karim et al., 2016; Marshall and Noireaux, 2018). However, there are limited examples of genetic circuits capable of dynamic, multi-gene regulation in CFS. CRISPRi-based genetic control is well established in CFS (Marshall and Noireaux, 2018; Westbrook et al., 2019). Incorporating CRISPRa into CFS could enable more facile circuit engineering by increasing the number of realizable network topologies (Figure S1) (Adler et al., 2017), and could overcome challenges that limit the utility of multi-layer CRISPRi repression circuitry in CFS.

A unique feature of CFS is that component turnover is greatly diminished compared with *in vivo* systems. CFS do not undergo dilution due to cell division and experience characteristically low protein and RNA turnover rates compared to cellular systems (Garamella et al., 2016). While component turnover can be accelerated via the addition of degradation machinery, this approach is inefficient and consumes valuable, finite resources (Garamella et al., 2016). In practice, this limited turnover makes repression circuits difficult to implement because even if transcription is halted the gene product is already present. In contrast, circuits based on activation are not dependent on turnover. Implementation of activation-based regulatory circuits would allow the high volumetric productivities resulting from limited component turnover to be combined with complex and dynamic multi-layer regulatory circuitry in a cell-free setting (Garamella et al., 2016). Thus, our first challenge was to adapt the CRISPRa system developed in *E. coli* for use in CFS. In this system, CRISPRa is applied using a 3′-extended guide RNA (scaffold RNA or scRNA) to direct dCas9 upstream of σ^{70} promoters. The 3′ extension of the guide RNA contains an RNA hairpin (MS2) which binds an RNA-binding protein (MCP) fused to a transcriptional activator (SoxS) (Figure 1A). In this system scRNAs encode information for targeting of dCas9 to precise locations along DNA as well as recruitment of a functional effector (Dong et al., 2018; Fontana et al., 2020; Kiattisewee et al., 2021; Zalatan et al., 2015). These scRNAs, J106, J206, and J306, are targeted via the spacer sequence directing CRISPRa to an expandable set of orthogonal synthetic promoters J1, J2, and J3 (Fontana et al., 2020).

To understand the portability of the CRISPRa system between *E. coli* and CFS, we tested whether basal expression levels and gene activation in CFS corresponded to previously observed trends in *E. coli*. In cells, CRISPRa can produce high levels of gene expression from a broad range of promoter strengths, but the fold activation decreases as basal promoter strength increases. We tested a set of synthetic minimal promoters (BBa_J231XX) (Figure S2) of varying strength in CFS. We observed a high correlation between CFS and *E. coli* for both basal promoter strength and fold activation by CRISPRa, providing Spearman correlation coefficients of 0.91 and 0.88, respectively (Figure S3). This observed correspondence between component function in *E. coli*-derived CFS and *E. coli* is consistent with previous reports (Garamella et al., 2016; Marshall et al., 2018; Shin and Noireaux, 2012), allowing exchange of individual genetic components between the two systems.

from the node. The expression of a small guide RNAs (sgRNAs), which lack the MS2 hairpin, targeted to the coding sequence (CDS) results in CRISPR transcriptional repression (CRISPRi) from the node.

(B) Schematic of CRISPRa/i circuits. CRISPRa/i nodes can be combined to form multi-layer CRISPRa/i networks when the guide RNA output generated by one node directs CRISPRa or CRISPRi at one or more other nodes in the network.

(C) Schematic presentation of CRISPRa/i genetic components for use in a cell-free system (CFS). CRISPRa/i system components are encoded on individual plasmids and assembled into networks by mixing with *E. coli*-derived CFS.

(D) Time course of CRISPRa in CFS. Left: CRISPRa-directed red fluorescent protein expression levels (mRFP1) from the J3 promoter are plotted as a function of time and J306 scRNA plasmid concentration. Right: Relative CRISPRa-directed RFP production rates (CRISPRa-directed production rates divided by unregulated production rates, STAR Methods) are plotted as a function of time and J306 scRNA plasmid concentration. Dashed line represents 2-fold activation compared with the basal expression control (0 nM J306 scRNA plasmid). Values represent the mean ± standard deviation of three technical replicates.

(E) Time course of CRISPRi in CFS. Left: CRISPRi-directed repression of green fluorescent protein (sfGFP) expression is plotted as a function of time and SF1 sgRNA plasmid concentration. SF1 targets the sfGFP CDS. Right: relative GFP production rates are plotted as a function of time and SF1 sgRNA plasmid concentration. Dashed line represents 50% repression compared with the basal expression control (0 nM SF1 sgRNA plasmid). Values represent the mean ± standard deviation of three technical replicates.

Next, we sought to formalize a framework for the construction of higher order CRISPRa/i circuits operating through interconnected CRISPRa/i nodes (Figure 1B). In this framework, CRISPRa/i nodes are discrete transcriptional units containing target sequences for CRISPRa- and/or CRISPRi-directed transcriptional regulation (Figure 1A). To characterize CRISPRa/i nodes, we isolated dCas9, sc/sgRNAs, and the MCP-SoxS activator onto individual plasmids (Figure 1C), allowing independent titration of expression levels for all CRISPRa/i components. CRISPRa/i node characterization is conducted by measuring the output response of each node to varying levels of component transcriptional inputs provided by titrating component plasmid concentrations. We found that increasing the concentration of sc/sgRNA-expressing plasmid resulted in higher overall levels of activation and repression (Figures 1D and 1E), as well as faster control (Figure S4). Titrations of dCas9-expressing plasmid revealed no differences in the strength of CRISPRa across a 40-fold range of dCas9 expression levels generated by 0.05 to 2 nM dCas9-expressing plasmid (Figure S5, left), likely due to saturation of active CRISPRa complexes at these concentrations of DNA target. For all levels of dCas9 expression, we observed a ~40 min delay between initiation of the cell-free reaction and the onset of CRISPRa/i control, consistent with the previously reported time of dCas9 maturation and CRISPR complex formation in CFS (Marshall et al., 2018; Westbrook et al., 2019). Titrations of plasmid expressing MCP-SoxS revealed a relatively wide region between 1 nM and 24 nM over which no significant differences in endpoint measurements of CRISPRa-mediated outputs were observed (Figure S5, right). Expression levels for dCas9 and MCP-SoxS activator were held constant throughout the work at 2 and 4 nM plasmid concentrations respectively.

Tuning CRISPRa/i through the regulated expression of guide RNAs in CFS

The ability to easily vary plasmid concentration in CFS, combined with the multi-component nature of CRISPRa/i regulatory complexes (Figure 1C), enables tuning of all component expression levels independently. Some tuning actions are global, for instance, varying dCas9 expression levels impacts both CRISPRa and CRISPRi. Other tuning actions, such as varying the level of activator protein, are expected to influence scRNA-mediated activation but not sgRNA-mediated repression. Likewise, output levels for individual nodes in a circuit can be linearly scaled by changing the concentration of plasmid at that node (Figure 1B). To provide simultaneous and independent control over both timing and expression levels of multiple target genes, we tuned CRISPRa/i control actions through the regulated expression of guide RNAs. Here, the specificity provided by guide RNA targeting allows tuning actions to be applied locally to individual CRISPRa/i nodes.

To quantify time-varying CRISPRa/i-directed changes in gene expression, we calculated production rates of CRISPR-regulated RFP expression relative to unregulated, basal expression of RFP (relative RFP production rate). At saturating levels of scRNA expression, CRISPRa achieved constant levels of activation over the course of 4–6 h providing a ~20-fold ± 2-fold increase in RFP production rate relative to an off-target control (Figure 1D, right). Likewise, relative production rates from CRISPRi with saturating levels of sgRNA (Figure 1E, right) achieved steady-state levels of repression by 3 h. Guide RNA titrations revealed that increasing levels of scRNA decreased the time to 2-fold activation by CRISPRa by up to ~5 h, and increasing levels of sgRNA decreased the time to 50% repression by CRISPRi by up to ~10 h (Figure S4, left). We found that sgRNA titrations were able to significantly affect the overall timing of gene expression as determined by the time to half maximum endpoint RFP values, with strong CRISPRi providing a ~3-h shift to earlier time points as compared with a no sgRNA control (Figure S4, right). Qualitatively, we observed that increasing sgRNA expression levels resulted in a higher fraction of total expression occurring at early time points. In contrast, scRNA titrations primarily provided a scaling factor to CRISPRa output levels without greatly affecting the timing of expression (Figures 1D and 1E, right; Figure S4, right). These data suggest that under these conditions CRISPRa kinetics may be dominated by the time required for MCP-SoxS expression and maturation.

Level-matching of multi-layer CRISPR circuitry in CFS

To enable the construction of multi-layer circuits, we built activation and activation-repression cascades by level-matching the input/output dynamic ranges between sequential CRISPRa/i nodes. That is, we matched the output transcription levels of an upstream node encoding scRNA to the relevant transcriptional input range of a downstream node encoding another sc/sgRNA. From sc/sgRNA plasmid titrations, we observed that both CRISPRa and CRISPRi respond to changes in input guide RNA expression levels spanning approximately 2 orders of magnitude (Figures 2A and 2C). Across this responsive range of sc/sgRNA inputs, CRISPRa-controlled outputs vary by ~24-fold at endpoint. While the dynamic range of CRISPRa generated outputs does not fully span the dynamic range of sc/sgRNA inputs, this characterization suggests that CRISPRa/i nodes can be sequentially combined by careful matching of upstream output ranges to downstream input ranges to form layered operations.

By tuning the concentration of plasmid expressing sc/sgRNA in the second layer of the cascades we were able to control the degree of overlap between response curves of upstream and downstream layers in the circuit. Based on the scRNA dose-response curves for CRISPRa by two different scRNAs in isolation (Figure 2A), we decided to build CRISPR activation-activation cascades to probe the composability of CRISPRa circuits from components characterized in isolation. Using these curves, we predicted how a 24-fold increase in transcription provided by CRISPRa in the first layer of the cascade affects cascade output. We made this prediction for four different concentrations of plasmid expressing scRNA in the second layer (Figure 2B). Upon construction of these CRISPRa cascades, we observed a strong agreement ($R^2 = 0.985$) between measured and predicted fold increases in outputs of CRISPRa cascades (Figure 2B). As expected, overlap between layers was maximized at 2-nM scRNA plasmid in the second layer, with the cascade providing a 16.3 ± 3.0-fold increase in measured RFP at endpoint compared with CRISPRa alone. Both lower, 0.5 nM, and higher, 4 nM, concentrations of scRNA-expressing plasmid in the second layer of the cascade resulted in decreased fold changes in cascade output, at 7.6 ± 0.6-fold and 15.2 ± 2.3-fold, respectively. From these data, we calculated the efficiency of signal propagation through the activation cascade by comparing the

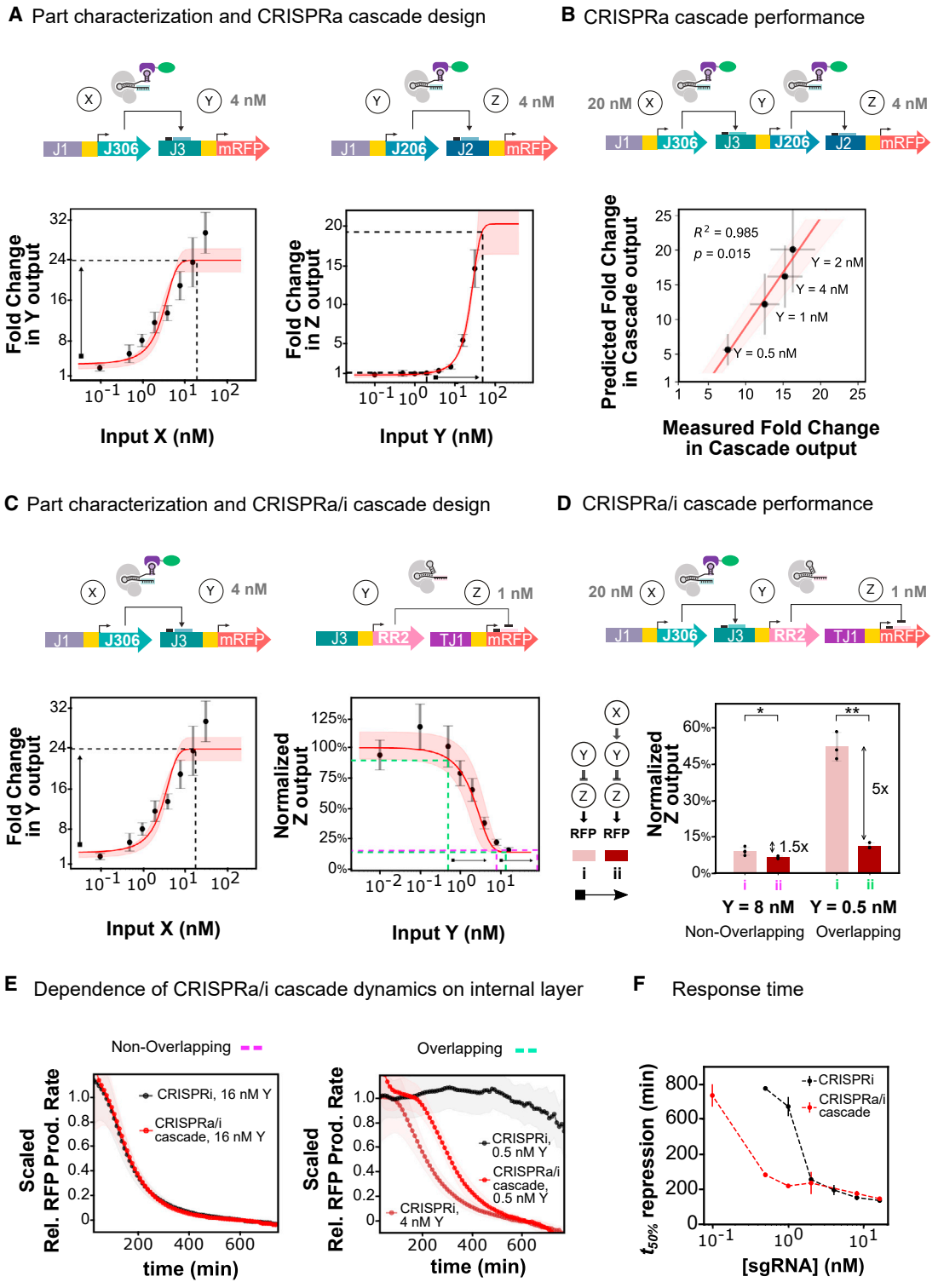

Figure 2. Level-matching enables construction of multi-layer CRISPRa/i circuits in CFS

(A) CRISPRa transcriptional input-output response curves. Top: expression of J306 scRNA (X) directs CRISPRa from the J3 promoter (Y) producing an RFP output. Expression of J206 scRNA (Y) directs CRISPRa from the J2 promoter (Z), producing an RFP output. Bottom: fold change in transcriptional output is plotted as a function of transcriptional input, specified by the scRNA plasmid concentration. Fold change is calculated as the ratio of RFP expression level at the reaction endpoint in the presence versus the absence of scRNA plasmid. Red line indicates a logistic fit to the data. Bottom right: pink and green dashed lines are guides showing the predicted effect of 25-fold increases in scRNA transcriptional input generated by CRISPRa in the first layer on the output of CRISPRa in the second layer of a two-layer activation cascade. Values represent the mean ± standard deviation of three technical replicates.

(legend continued on next page)

observed fold change in cascade output to the fold change provided by CRISPRa in the input layer. Currently, given optimal level-matching, we observe 67.9% ± 18.1% signal propagation for the two-layer CRISPRa cascade. Together, these results suggest that we can predictably tune the degree of overlap between layers of CRISPRa/i circuits to propagate signals, satisfy input requirements of potential downstream layers, and tailor absolute gene expression levels.

Next, we constructed an activation-repression cascade with CRISPRa in the input layer activating transcription of RR2 sgRNA, which targets the coding sequence of *mrfp1* for CRISPRi in the second layer of the cascade (Figure 2D, top). As in construction of the activation-activation cascade, level-matching was informed by the sc/sgRNA dose-response curves for CRISPRa and CRISPRi obtained in isolation (Figure 2C). As expected, when the overlap between layers was maximized, the CRISPRa/i cascade generated 4.6-fold ± 0.7 more repression than CRISPRi alone (Figure 2D, right). The importance of matching upstream outputs to the responsive range of downstream inputs was illustrated by overexpression of sgRNA in the second layer of the activation-repression cascade, intentionally minimizing the overlap between the upstream and downstream layers of the cascade. Under these conditions, the activation-repression cascade reduced RFP expression by 1.4-fold ± 0.3 compared with CRISPRi (Figure 2D, left).

CRISPRa/i circuits encode dynamic gene expression programs

Next, we sought to investigate the ability of multi-layer CRISPRa/i circuitry to encode dynamic gene expression programs inaccessible to simpler single-layer controllers. As a first step, we explored the influence of level-matching on CRISPRa/i cascade dynamics by comparing relative RFP production rates arising from an activation-repression cascade with those generated by CRISPRi. When there was a high degree of overlap between the response curves of the layers in the cascade, significant changes in the timing of gene expression were observed (Figures 2E, right, and 2F). For instance, an activation-repression cascade with 0.5 nM of sgRNA plasmid resulted in repression of the RFP output at a comparable rate but delayed onset compared with that of CRISPRi repression alone with 4 nM of sgRNA plasmid. This delay is interpreted as the time required for CRISPRa to activate sgRNA expression in the second layer of the circuit. We identified a ~10-fold range of sgRNA plasmid concentrations over which a CRISPR activation-repression cascade could generate significant differences in expression dynamics compared with single-layer CRISPRi (Figure 2F).

As expected, when sgRNA expression levels were mismatched, we observed negligible differences in expression dynamics. If the concentration of plasmid expressing sgRNA in the second layer of the activation-repression cascade was too low, e.g., 0.01 nM, no repression was observed. Conversely, high concentrations of sgRNA-expressing plasmid in the second layer of the cascade effectively resulted in CRISPRi applied in a single layer, producing expression dynamics identical to that of the CRISPRi control (Figure 2E, left). Above 2 nM of sgRNA-expressing plasmid, we observed no difference in the time to 50% repression for the CRISPRa/i cascade as compared with single-layer CRISPRi (Figure 2F). Together, these results underscore that gene expression dynamics can be tuned by multi-layer CRISPRa/i circuits when there is sufficient overlap between the response curves of the CRISPRa/i circuit components.

After establishing the rules governing construction of layered CRISPRa/i circuitry, we endeavored to create more complex transcriptional programs to explore the scalability and composibility of CRISPRa/i regulatory networks. We combined the CRISPR activation-repression cascade with CRISPRa to form

(B) Two-layer CRISPRa cascade. Top: Expression of J306 scRNA at node X directs CRISPRa from the J3 promoter at node Y. Expression of J206 scRNA from the J3 promoter (Y) directs CRISPRa from the J2 promoter, which expresses mRFP1 (Z). Bottom: scatter plot comparing measured and predicted fold change in cascade output. The measured fold change in cascade output is calculated as the ratio of measured RFP outputs with and without CRISPRa in the first layer of the circuit (STAR Methods) and are presented as the mean ± standard deviation of three technical replicates. Predicted cascade fold changes and uncertainties are calculated from the fits to the scRNA plasmid titrations shown in 2A. Statistical significance of non-zero slope was calculated using two-tailed unpaired Welch's t-test.

(C) CRISPRa/i transcriptional input-output response curves. Top: expression of J306 scRNA (X) directs CRISPRa from the J3 promoter (Y), producing an RFP output. Expression of the RR2 sgRNA (Y) directs CRISPRi of mRFP1 (Z). Bottom: fold change in transcriptional output is plotted as a function of transcriptional input, specified by the scRNA and sgRNA plasmid concentration. Red line indicates a logistic fit to the data. Bottom left: response curve for J306 scRNA presented as in 2A Bottom right: CRISPRi data are represented as percent expression of a no repression control (STAR Methods). Pink and green dashed lines show the expected effect of a 25-fold increase in sgRNA transcription provided by CRISPRa in the first layer on the CRISPRi-directed output in the second layer of a two-layer CRISPR activation-repression cascade. Values represent the mean ± standard deviation of three technical replicates.

(D) Two-layer CRISPRa/i cascade. Top: expression of J306 scRNA (X) directs CRISPRa from the J3 promoter. RR2 sgRNA expression from the J3 promoter (Y) directs CRISPRi of mRFP1 (Z). Bottom: percent of maximum expression is calculated as in Figure 2C comparing CRISPRi in one layer (I, light red) to two-layer CRISPR activation-repression cascades (II, dark red) at two different concentrations of sgRNA in the second layer. Values represent the mean ± standard deviation of three technical replicates. Asterisks indicate a statistically significant difference using a two-tailed unpaired Welch's t-test (*p value < 0.05, **p value < 0.01, ***p value < 0.001).

(E) CRISPRi and CRISPRa/i circuit dynamics. Left: gene expression over time for RFP controlled by CRISPRi and CRISPRa/i cascade at a concentration of plasmid Y that falls outside the range where input-output levels between the first and second layers overlap (no level-matching). Black line represents the scaled relative RFP production rate due to CRISPRi with 16 nM of plasmid encoding RR2 sgRNA while the red line represents the scaled relative RFP production rate generated when CRISPRa is applied to the same concentration of sgRNA plasmid. Right: comparison of CRISPRi and CRISPRa/i cascade at a concentration of plasmid Y that permits level-matching between the first and second layers of the circuit. Black line represents the scaled relative RFP production rate generated by CRISPRi with 0.5 nM of plasmid encoding RR2 sgRNA while the red line represents expression generated when CRISPRa is applied to the same concentration of sgRNA plasmid. The dark red line shows the scaled relative expression generated by CRISPRi with 4 nM of sgRNA plasmid and is provided as a point of reference. Data are presented as mean ± standard deviation of three technical replicates.

(F) Time to 50% repression is plotted against the concentration of sgRNA plasmid for both CRISPRi (black line) and a CRISPRa/i cascade (red line). Showing that when output/input ranges of the first and second layers overlap, multi-layer CRISPRa/i circuits can be used to tune the timing of gene expression. Data are presented as mean ± standard deviation of three technical replicates.

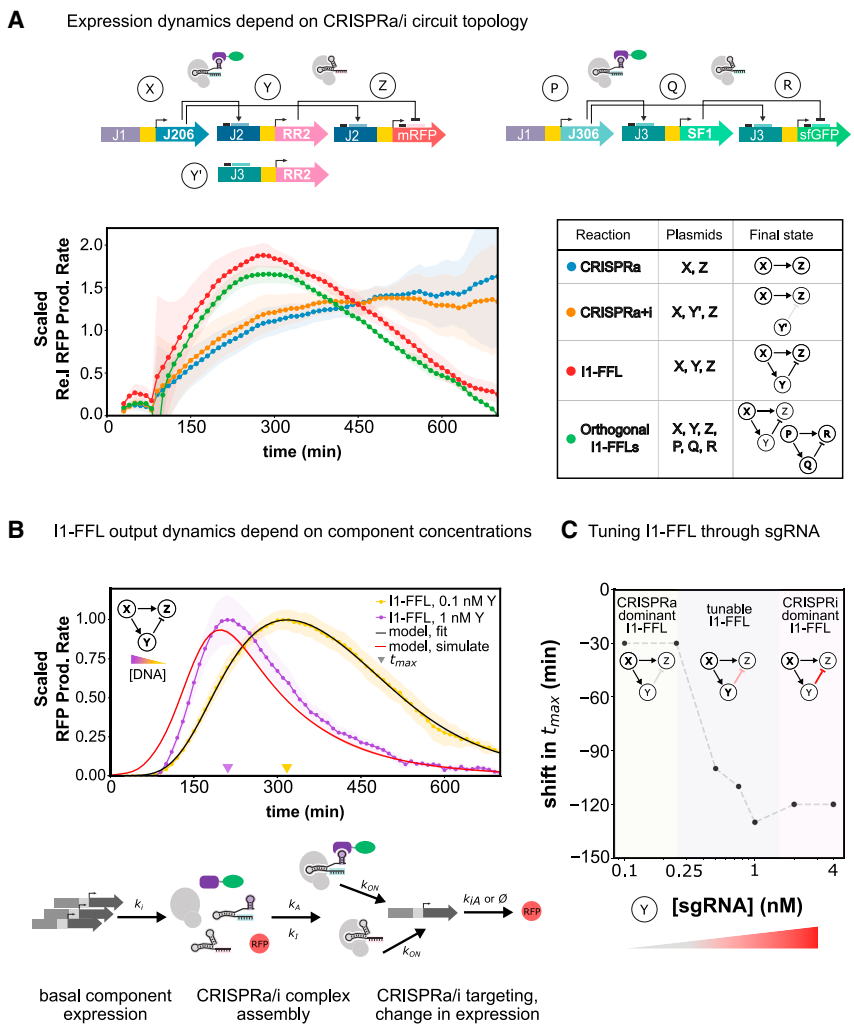

Figure 3. Programing distinct multi-layer CRISPRa/i circuit dynamics in CFS

(A) Time course for four different CRISPRa/i networks including orthogonal type-1 incoherent feed forward loops (I1-FFL) operating in CFS. Normalized relative RFP production rates are plotted as a function of network topology, as indicated. Outputs are scaled by the respective endpoints to fit on a common axis. Values represent the mean ± standard deviation of three technical replicates.

(B) Time course for I1-FFL variants shows dependence of output expression dynamics on sgRNA concentration. Scaled RFP production rates are plotted as a function of time for two different RR2 sgRNA plasmid concentrations; 0.1 and 1 nM shown in yellow and purple, respectively. Fits to the illustrated I1-FFL are used to predict expression dynamics as a function of sgRNA concentration. The model fit to the measured 0.1 nM data is shown in black, and the model prediction for expression dynamics from an I1-FFL with 1 nM sgRNA-expressing plasmid is shown in red. Yellow and purple triangles along the x axis denote the time of maximal expression of the pulse generated by the I1-FFL. Values represent the mean ± standard deviation of three technical replicates.

(C) Shift in time of the I1-FFL expression maxima depends on sgRNA plasmid concentration, which controls the strength of the CRISPRi connection between nodes Y and Z. The time at which the maximum output rate is achieved (t_{max}) is plotted as a function of RR2 sgRNA plasmid concentration, which is expressed from node Y and acts on node Z.

an incoherent type-1 feedforward loop (I1-FFL), a classic pulse generating circuit that is significantly overrepresented in natural systems (Alon, 2007; Kaplan et al., 2008; Mangan and Alon, 2003; Shen-Orr et al., 2002). When level-matching is taken into consideration, we see that circuit topology determines the timing of gene expression (Figure 3A). As expected, we observed no difference in expression dynamics between CRISPRa and CRISPRa + CRISPRi (CRISPRa+i) at low concentrations of sgRNA-expressing plasmid (Figure 3A, blue, orange). When expression of sgRNA at node Y was activated by CRISPRa to form an I1-FFL (Figure 3A, red), we observed a gene expression pulse, qualitatively different from expression generated by CRISPRa or CRISPRa+i. Upon addition of an orthogonal I1-FFL controlling expression of GFP to the same reaction (Figure 3A, green), no differences in the timing of gene expression were observed at the output of the RFP I1-FFL. This result indicates that we can operate multiple circuits simultaneously without compromising the respective expression dynamics.

We were able to tune the timing of the gene expression pulse generated by the I1-FFL by varying the concentration of sgRNA-expressing plasmid. The maximum RFP production rate occurred ~110 min earlier in the cell-free reaction when we increased the sgRNA-expressing plasmid concentration 10-fold from 0.1 to 1 nM (Figure 3B). More generally, we observed that the time of the maximum gene expression pulse could be continuously tuned over a 4-fold change in sgRNA plasmid levels, shifting expression maxima earlier by up to 2 h compared with unregulated expression (Figure 3C). To capture the I1-FFL expression dynamics and evaluate the feasibility of rationally tuning CRISPRa/i circuits *in silico*, we constructed a coarse-grained mechanistic model of CRISPRa/i gene regulation (Choi et al., 2018; Medley et al., 2018). We defined first-order chemical reactions for protein and guide RNA production, CRISPR complex assembly, and DNA targeting (Figure 3B, bottom; Table S3). When an initial experimental observation was provided, the model was capable of predicting the effects of tuning actions applied to the I1-FFL on gene expression dynamics (Figure 3B, fit and simulate). Here, the model is fit to the experimental data for an I1-FFL with 0.1 nM sgRNA-expressing plasmid and used to predict the expression dynamics for an I1-FFL with 1 nM sgRNA-expressing plasmid. Similar results were obtained when fitting to the 1 nM condition and predicting the 0.1 nM condition (Figure S8). We observed a ~10-min difference between the measured and predicted timing of maximum RFP production rate, corresponding to the time resolution of our measurements. Combined with the observed predictability of level-matching in CRISPRa/i

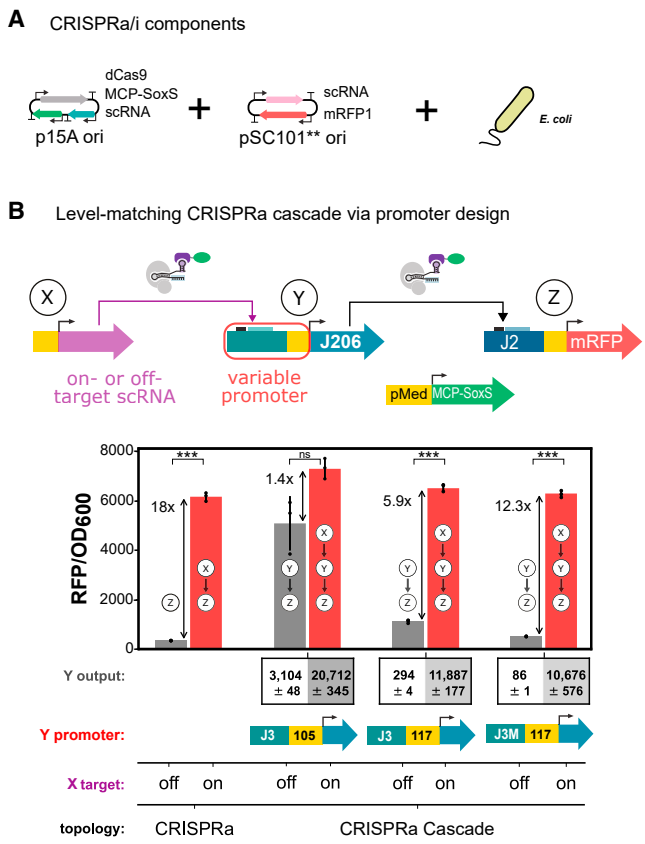

Figure 4. Level-matching of CRISPRa cascades in *E. coli*

(A) Schematic of CRISPRa genetic components and assembly to form CRISPRa circuits in *E. coli*. Circuits are assembled by transformation of different combinations of plasmids into *E. coli*. Activator, dCas9, and scRNAs in the first layer of a circuit are expressed from a p15A plasmid while reporters and scRNAs in the second layer of a circuit are expressed from a pSC101** origin of replication plasmid. Data are collected in *E. coli* MG1655 grown overnight at 37°C with shaking in EZ MOPS with 0.2% glucose and appropriate antibiotic selection.

(B) Top: schematic of CRISPRa cascade. Tuning actions are applied by changing expression characteristics of the activatable promoter in the second layer of the circuit. Bottom: CRISPRa on the J2 promoter is compared with the output at node Z of the activation cascade with (red bars) and without (gray bars) input provided by node X. Y output denotes the expression levels obtained at node Y in the presence and absence of input activation from X for the tuning variant provided by Y promoter. Data are represented as mean ± standard deviation of RFP/OD_{600}. Asterisks indicate a statistically significant difference using a two-tailed unpaired Welch's t_test (*p value < 0.05, **p value < 0.01, ***p value < 0.001).

cascades, these results suggest that high-fidelity CRISPRa/i circuits could be designed and tuned *in silico* given component characterization data.

CRISPRa/i circuits in *E. coli*

To form dynamic, multi-layer circuitry in *E. coli*, CRISPRa/i circuits are encoded on two plasmids. One plasmid contains dCas9, MCP-SoxS, and scRNAs acting as inputs to the first layer of a circuit, while the second plasmid contains a fluorescent reporter as well as sc/sgRNAs acting in the second layer of a circuit (Figures 4A and 5A). Unlike cell-free systems, in which the expression level of every circuit component can be precisely titrated, gene expression in cells is constrained by the expression levels achievable given different combinations of plasmid copy number and genetic parts. Level-matching of multi-layer CRISPRa/i circuits in cells is therefore more challenging and requires attention not only to the dynamic range of components but also the absolute expression levels and activities.

Level-matching in multi-layer CRISPRa circuits

To understand the level-matching requirements of scRNAs in multi-layer CRISPRa cascades in *E. coli*, we engineered the basal expression characteristics of CRISPRa nodes in the second layer of a two-layer activation cascade. In this circuit, scRNA expressed at node X targets CRISPRa to a promoter at node Y, activating expression of a second scRNA, targeting a fluorescent reporter at node Z for CRISPRa. Tuning of basal expression levels was accomplished through the use of synthetic minimal promoters (BBa_J231XX), as well as modifications to the 5′ sequence proximal to the minimal promoter at node Y, driving scRNA expression in the second layer (Figure 4B). At the highest basal levels of scRNA expression in the second layer, CRISPRa cascades yielded 1.4x higher output levels than a comparable single-layer circuit. Decreasing basal scRNA expression levels in the second layer of the cascade by ~10x increased the output dynamic range of the CRISPRa cascade to 5.9x. Decreasing basal scRNA expression levels by a further 3.4x increased the output dynamic range by an additional 2x, resulting in an overall activation ratio of 12.3x for the CRISPRa cascade as compared with the single-layer circuit. Output levels of CRISPRa cascades at all tested scRNA expression levels were comparable with output of single-layer CRISPRa with saturating levels of scRNA expression. We observed that CRISPRa cascades were sensitive to scRNA expression, with 32% compression of the output dynamic range observed even at the lowest basal expression level of scRNA at node Y. Compression of the output dynamic range in cascades can be attributed to basal scRNA expression in the second layer of the circuit. These results suggest that engineered promoters capable of lower basal scRNA expression levels would minimize compression of activation cascade dynamic ranges.

Inducible CRISPRa by expressing MCP-SoxS from an inducible promoter

To provide an input for dynamic CRISPRa/i circuitry in *E. coli*, we chose to apply control over CRISPRa through inducible expression of the MCP-SoxS activator protein (Figure 5B). We observed that output levels generated by CRISPRa were titratable through aTc induction of MCP-SoxS activator (Figure 5B, right). These output levels were similar to CRISPRa employing constitutive expression of MCP-SoxS (Figure 4B, left) as well as aTc induction of scRNA (Figure S9, left). Compared to CRISPRa with constitutively expressed activator and off/on-target scRNA, the aTc-inducible system provided 40% lower basal levels and 16.5% lower activated levels of reporter expression (Figure 5B). A 40.4 ± 0.77-fold increase in expression was observed for the constitutive CRISPRa system supplied with on versus off-target scRNAs, whereas aTc induction of MCP-SoxS with on-target scRNA yielded a 56.3 ± 0.65-fold increase. A similar, 43-fold increase was observed when comparing aTc-inducible MCP-SoxS with on/off-target scRNA (Figure S9, right). Together, these results establish aTc-inducible expression of the MCP-SoxS activator as a means of generating titratable levels of activation.

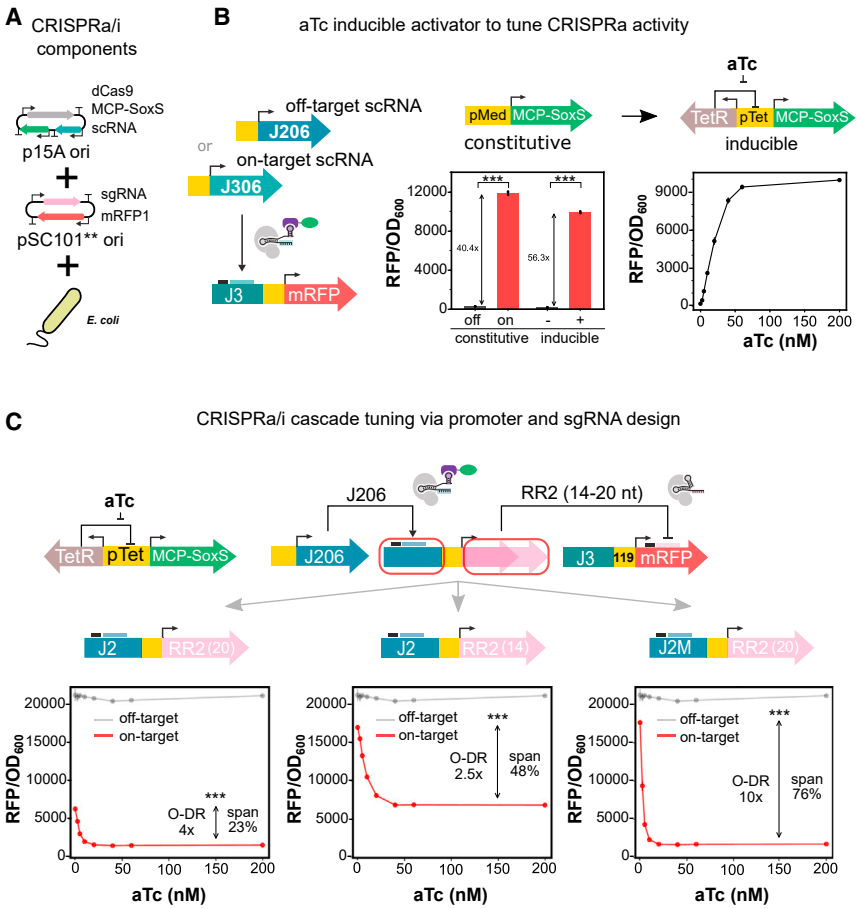

Figure 5. Level-matching of CRISPRa/i cascades in *E. coli* with titratable input

(A) Schematic of CRISPRa/i genetic components and assembly to form CRISPRa/i circuits in *E. coli*. Circuits are assembled by transformation of different combinations of plasmids into *E. coli*. Activator, dCas9, and scRNAs in the first layer of a circuit are expressed from a p15A plasmid while reporters, and sc/sgRNAs in the second layer of a circuit are expressed from a pSC101** origin of replication plasmid. Inducible CRISPRa/i data are collected in *E. coli* MG1655 grown O/N, diluted 1:40, grown for 3 h, and diluted 1:40 into inducing media, all at 37°C with shaking in EZ MOPS with 0.2% glucose and appropriate antibiotic selection.

(B) Dependence of CRISPRa on aTc-induced MCP-SoxS expression. Left: circuit schematic showing how inducible CRISPRa is provided by pTet controlled expression of MCP-SoxS activator. For both constitutive and inducible CRISPRa, J306 scRNA directs dCas9 to the J3 promoter. Constitutive CRISPRa is compared with on/off-target scRNA while inducible CRISPRa is compared ± inducer with on-target scRNA. Center: mRFP1 output of aTc-inducible CRISPRa ± aTc is compared with constitutive CRISPRa with on/off-target scRNA. Data are represented as mean of measured RFP/OD_{600} ± standard deviation of three biological replicates. Right: aTc induction of activator protein provides titratable levels of activation. Data are represented as the mean ± standard deviation of measured RFP fluorescence/OD_{600} for three biological replicates. Asterisks indicate a statistically significant difference using a two-tailed unpaired Welch's t-test (*p value < 0.05, **p value < 0.01, ***p value < 0.001).

(C) Two-layer CRISPRa/i cascade output dependence on promoter and sgRNA. Top: schematic of aTc-inducible CRISPRa activating expression of sgRNA targeting mRFP1 for CRISPRi. Level-matching is achieved through engineering basal expression characteristics of the activatable promoter driving sgRNA expression as well as through modifications of sgRNA activity via 5′ sgRNA truncations that reduce sgRNA spacer-target DNA complementary from 20 to 14 nucleotides. Bottom: CRISPRi response to increasing levels of activation of the promoter driving sgRNA expression for three different tunings. On-target sgRNA is plotted in red while off-target sgRNA is plotted in gray. Data are represented as mean RFP/OD_{600} ± standard deviation. Calculations for span and output dynamic range (O-DR) can be found in STAR Methods. Asterisks indicate a statistically significant difference using a two-tailed unpaired Welch's t-test (*p value < 0.05, **p value < 0.01, ***p value < 0.001).

Level-matching of multi-layer CRISPRa/i circuits in E. coli

To understand the level-matching requirements of sgRNAs in multi-layer CRISPRa/i circuits in *E. coli*, we constructed an inducible CRISPR activation-repression cascade. Here, we titrated the CRISPRa input in the first layer and tuned both the expression characteristics of the promoters and the activities of sgRNAs in the second layer of the cascade. Tuning of CRISPRa inputs in the first layer of the cascade was provided by the previously described inducible MCP-SoxS activator system. In the second layer of the cascade, expression characteristics of promoters were tuned via modifications to the 5′ sequence proximal to the minimal promoter, while sgRNA activities were modified through the use of 5′ spacer truncations (Fontana et al., 2018b; Qi et al., 2013) (Figures 5C and S11). When the J2 promoter was used to express RR2 sgRNA targeting RFP (Fontana et al., 2018b), we observed 70% repression in the absence of activation (Figure 5C, left). A ~20-fold increase in sgRNA expression provided by CRISPRa (Figure S10) resulted in an output dynamic range of 4-fold, spanning 23% of accessible expression levels. Decreasing the strength of CRISPRi via truncation of the RR2 sgRNA spacer to 14 nucleotides decreased repression in the absence of activation of sgRNA expression to 20% as compared with an off-target control. However, truncated guide RNAs were not able to achieve high levels of repression at maximal levels of activation (Figure 5C, center) resulting in a compressed output dynamic range of 2.5-fold, spanning 48% of accessible expression levels. Tuning of sgRNA expression levels via modifications to the 5′ sequence proximal to the minimal promoter resulted in 17% and 92% repression in the absence and presence of CRISPRa applied to RR2 sgRNA, respectively, yielding an output dynamic range of ~10-fold, spanning 76% of the accessible expression space (Figure 5C, right). Taken together, the inducible CRISPRa/i cascade and the CRISPRa cascade indicate that guide RNA expression levels produced by CRISPRa are sufficient to saturate downstream layers of CRISPRa/i circuits, and that both CRISPRa and CRISPRi are highly sensitive to basal expression of sc/sgRNAs.

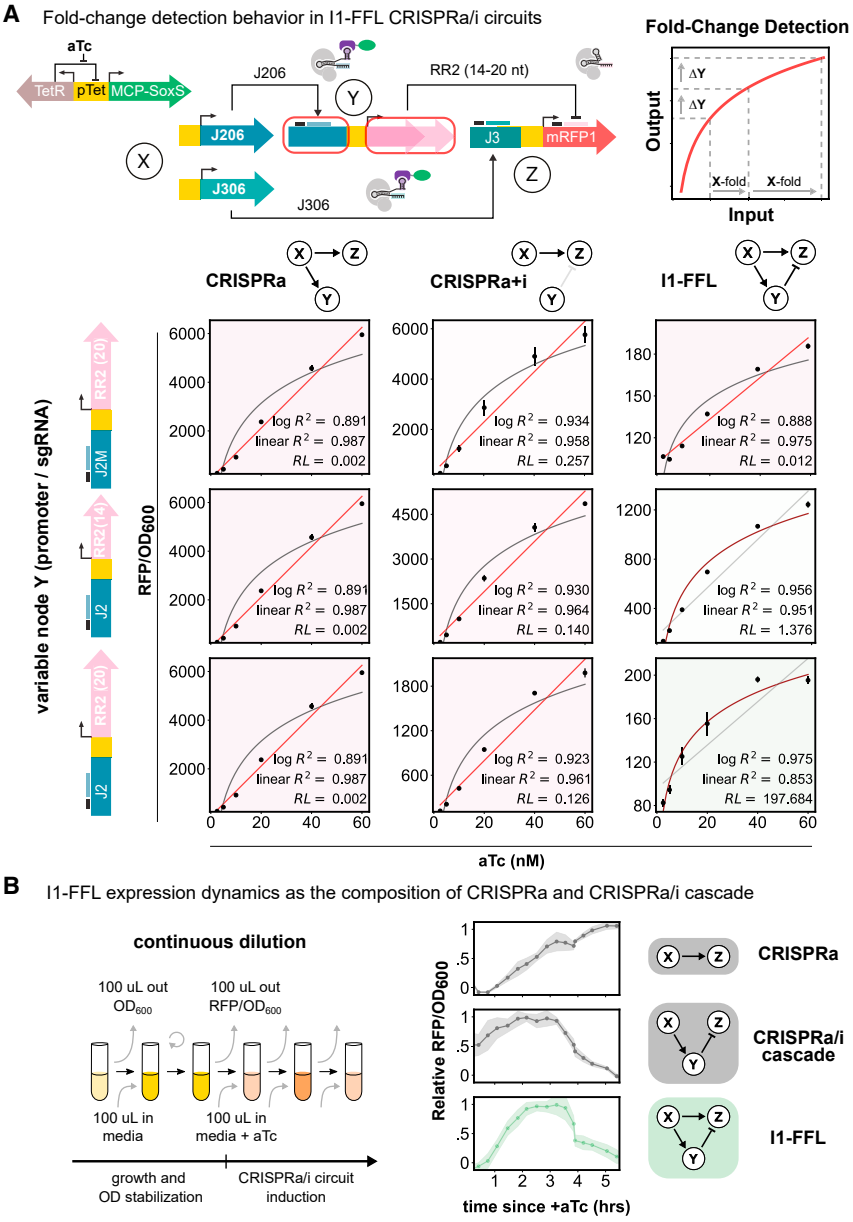

Figure 6. Tunable and composable dynamic CRISPRa/i circuits in *E. coli*

(A) Fold-change detection behavior in I1-FFL CRISPRa/i circuits. Top: circuit schematic of CRISPRa/i incoherent type 1 feedforward loop (I1-FFL) implemented in *E. coli*. Here, tuning of repression by node Y is achieved by changes to the transcriptional properties of the promoter at node Y or through modifications to the sgRNA expressed at node Y. aTc induction of MCP-SoxS activator serves as a titratable input to the system. At right, a graphical definition of fold-change detection: the same fold change in input "X" produces the same change in output "Y." Bottom: aTc response for 9 combinations of network topology and sgRNA tuning showing that connectivity between nodes and tuning specifies input/output relationship of complex CRISPRa/i circuits. Network topologies are indicated along the top while tuning variants are represented along the left. Grayed out arrow in CRISPRa+I indicates on-target sgRNA from an unactivated promoter. I1-FFLs must have specific component relationships to achieve fold-change detection seen here as logarithmic input/output response curves. Data are represented as the mean of measured RFP/OD_{600} ± standard deviation of three biological replicates. Data for off-target sgRNA are the same in all three plots and is collected in the J2 context (bottom left). Statistical significance was assessed by calculating the relative likelihood (*RL*) of the log fit best describing the data as compared with the linear fit, STAR Methods.

(B) CRISPRa/i circuit expression dynamics were measured in a continuous dilution experiment. Left: schematic of continuous dilution experimental design and procedure. Right: Expression dynamics of CRISPRa, CRISPRa/i cascade, and an I-1FFL tuned for fold-change detection are compared. Data are presented as relative RFP/OD_{600} ± standard deviation of three biological replicates (STAR Methods). For CRISPRa and the IFFL, RFP is expressed from the standard J3 reporter with a BBa_J23117 minimal promoter while for the CRISPRa/i cascade the strong minimal promoter BBa_J23119 is used to enable observation of inhibition in this assay. Relative RFP/OD_{600} scales data to the respective output response ranges to place them on a common scale for comparison of output expression dynamics.

Tunability of CRISPRa/i enables interrogation of complex behavior in E. coli

The ability to tune CRISPRa/i circuits through both promoter engineering and guide RNA truncations allows control over the abundance and strength of individual sc/sgRNAs. Such control enables independent tuning of nodes in multi-layer CRISPRa/i circuitry. Paired with the ease of circuit construction, the CRISPRa/i system is suited for rapid circuit function interrogation. To showcase multi-guide tuning and circuit function exploration, we constructed and characterized three different I1-FFLs in which application of repression by node Y was varied.

To enable observation of dynamic circuit behaviors and provide titratable levels of input activation, we chose to use inducible expression of the activator protein MCP-SoxS (Figure 5B). To understand the effect of tuning actions on I1-FFL output, we constructed three different network topologies (Figure 6A. top), an I1-FFL, CRISPRa+i, and CRISPRa with an off-target sgRNA. We compared the response of these three circuits to increasing levels of MCP-SoxS induction for three different tunings of sgRNA expression (Figure 6A, bottom). To determine how much of the repression in the I1-FFL could be attributed to the basal expression from node Y, we compared the CRISPRa+i circuit with CRISPRa with off-target sgRNA (Figure S12). We observed 7,500 RFU from CRISPRa+i with off-target sgRNA. CRISPRa+i expressing full-length on-target sgRNA from the J2 promoter provided 2,200 and 71 RFU at 200 nM and 0 nM aTc, respectively. Thus, basal expression of the sgRNA from node Y has the effect of reducing, or compressing, the output range of the MCP-SoxS CRISPRa titration by 70%. In an I1-FFL with the same sgRNA expression tuning, the output dynamic range

was only 3-fold (Figure S12). We reasoned that decreasing the strength of repression at node Z would reduce compression in the CRISPRa+i circuit and increase the dynamic range of the I1-FFL. Tuning repression through sgRNA truncation to 14 nt decreased compression of the output range by the CRISPRa+i circuit from 70% to 24% and increased the output dynamic range of the I1-FFL from 3- to 15-fold (Figure S12). Tuning repression through modifications to the sequence 5′ of the minimal promoter expressing sgRNA resulted in 4% compression of the output range by CRISPRa+i. However, counterintuitively the I1-FFL output dynamic range was decreased to 2-fold with the same modifications to the sequence 5′ of the minimal promoter expressing sgRNA (Figure S12). While the latter result was unexpected, the current suite of tuning actions available to the CRISPRa/i system in *E. coli* nonetheless does allow independent tuning of interactions between nodes in multi-guide circuits.

I1-FFLs are used in many naturally occurring sensory systems as fold-change detectors to generate dynamic outputs determined by relative, as compared to absolute, differences in inputs to the system (Adler and Alon, 2018). Formally, fold-change detection (FCD) can be defined as a logarithmic relationship between inputs "I" and outputs "O," i.e., an input/output response curve, satisfying the equation $O = a \cdot ln(I) + b$. Theoretical work has shown that a transcriptional I1-FFL is capable of FCD only under specific ratios of component expression levels and strengths (Goentoro et al., 2009). Experimentally, we can test for FCD in these circuits by evaluating the variance explained by a logarithmic fit to outputs taken as a function of aTc-induced MCP-SoxS inputs. Consistent with expectation, we observed that only I1-FFLs with specific sgRNA tunings were capable of detecting fold changes of aTc over the linear range of MCP-SoxS induction (Figure 5B, right). Over this linear range, we observed an R^2 of 0.975 for a logarithmic fit between the inputs and outputs, as compared with an R^2 of 0.853 for a linear fit to the data for the I1-FFL with 20nt RR2 sgRNA expressed from the J2 promoter (Figure 6A, bottom right). Using these R^2 values we can calculate Akaike information criterion scores (AICc) (STAR Methods) for each model. The relative likelihood of the data being described by a logarithmic as opposed to a linear model can then be computed using the AICc scores for each model. For the IFFL with RR2 sgRNA expressed from the J2 promoter, we find that the logarithmic model is 197 times more likely to describe the data than a linear one. We can extend the test for FCD beyond the linear range of aTc-induced MCP-SoxS inputs by converting these inputs into the corresponding CRISPRa responses. We linearized the CRISPRa response to aTc induction by dividing CRISPRa output levels at a given aTc induction level by the CRISPRa output at saturating concentrations of aTc. Plotting I1-FFL outputs against this percent induction of the CRISPRa response provided an R^2 of 0.989 for a logarithmic fit, as opposed to only 0.896 for a linear fit resulting in a relative likelihood of 880 for the data being described by a logarithmic model. By comparison, the corresponding CRISPRa+i circuit exhibited an R^2 for the input-output relationship of 0.852 for a logarithmic fit, and 0.997 for a linear fit resulting in a relative likelihood of less than 0.001 or, stated differently, the linear model is at least 1,000 times more likely than the logarithmic one to describe the observed data (Figure S13). Taken together, these data show that CRISPRa/i circuits assembled into I1-FFLs can be tuned to achieve FCD. This demonstrated capacity of CRISPRa/i circuits to perform non-linear mapping between inputs and outputs expands the utility of the CRISPRa/i system, allowing complex relationships to be encoded as network topologies.

To investigate the composability of CRISPRa/i-controlled gene expression dynamics, we tested three inducible circuits under continuous dilution: CRISPRa, an activation-repression cascade, and an I1-FFL tuned for FCD (Figure 6B, left). We observed increases in RFP/OD_{600} roughly 1 h post-induction for both the I1-FFL and CRISPRa corresponding to the action of the first layer in both circuits (Figure 6B, right). For both the I1-FFL and the activation-repression cascade, repression onset was observed at ~5 h, corresponding to the action of the second layer of each circuit. While I1-FFLs are recognized as a classic pulse generating circuit, in order to achieve FCD gene expression pulses must display perfect adaptation (Adler and Alon, 2018; Goentoro et al., 2009), meaning gene expression must return to the basal level after completing the pulse. Here, we observed an adaptive pulse of gene expression from the I1-FFL that starts at the baseline and ends at the baseline, corroborating the ability of the CRISPRa/i I1-IFFL to function as a fold-change detector. Overall, these results indicate that CRISPRa/i circuits are composable in that the observed dynamic behaviors can be understood from the functions of the parts.

DISCUSSION

We have developed a set of components and a unifying framework for building dynamic CRISPRa/i gene regulatory networks that are scalable, composable, and tunable. These networks are built from CRISPRa/i nodes, which we define as transcriptional units that can be targeted for regulation by both CRISPRa and CRISPRi. The CRISPRa/i framework leverages an expandable set of synthetic promoters and orthogonal guide RNAs to specify arbitrary transcriptional regulatory topologies. The characteristics and limitations of the network are therefore determined by the properties of the constituent components. Particularly, promoter dynamic range and guide RNA function specify the transcriptional input-output relationship of each node. Understanding these relationships will be fundamental for building deep, wide, and fast regulatory networks.

We can estimate the upper bound for the maximum depth of activation cascades based on the observed cascade performance in this work. At present we observe 68% ± 18% signal propagation in a two-layer activation cascade (Figure 2B). The total fraction of signal propagated in deeper cascades can be calculated by raising the fraction of signal propagated between two layers to the total number of internal layers in the cascade. This calculation indicates the current CRISPRa/i system in CFS can support cascades up to 6 layers deep before output activation ratios fall below 2.5-fold. Similarly, we achieved 68% ± 2.7% signal propagation in *E. coli* (Figure 4B), suggesting activation cascades of up to 6 layers could be built with the current implementation of the CRISPRa system *in vivo*. With the components presented in this work, transcriptional activation generated by CRISPRa does not fully span the input dynamic range of sc/sgRNA expression in downstream layers (Figure 2), resulting in degradation of signals as they are propagated through multilayer CRISPRa/i circuits. The most general solution to increase

fidelity of signal propagation in both CFS and *E. coli* is through engineering improved system components. Promoters with lower basal expression, leading to larger output dynamic ranges, would span a higher fraction of the input dynamic range of downstream nodes, resulting in less signal degradation between layers and deeper CRISPRa/i circuitry. We estimated that engineered promoters with a mere 5-fold increase in output dynamic range would allow CRISPRa-directed outputs to fully span the input dynamic range of sc/sgRNAs in downstream layers. In this system, modest improvements in signal propagation efficiency between layers would enable drastically deeper CRISPRa/i networks. For instance, increasing the fraction of signal propagated between layers by 12%, and output dynamic ranges by 2-fold would, in theory, enable cascades up to 14 layers deep before output activation ratios fall below 2.5-fold. While deeply layered cascades remain beyond the scope of current engineered regulatory networks, the large activation ratios and high fidelity of signal propagation observed in the CRISPRa/i system contribute to the robust operation of shallower networks.

Natural systems coordinate the expression of many outputs with few internal layers of computation using wide, highly interconnected networks such as dense overlapping regulons (Rosenfeld and Alon, 2003; Shen-Orr et al., 2002; Thieffry et al., 1998). Our results indicate the CRISPRa/i system is well suited to design of wide control circuits for simultaneous and independent multi-gene regulation. In CFS, CRISPRa levels and kinetics are unchanged with respect to scRNA expression across at least an order of magnitude (Figure S6). Additionally, RFP expression levels are unchanged over a ~40-fold range of dCas9 plasmid concentration (Figure S5). This indicates that the cell-free reaction has the resources to express high levels of scRNA and dCas9 without hindering system performance. Construction of two orthogonal I1-FFLs in the same reaction showcases the ability of CFS to harbor large circuits expressing many different sc/sgRNAs to execute multiple independent programs simultaneously. Likewise, *E. coli* are capable of expressing high levels of sc/sgRNA without experiencing growth defects or retroactivity due to guide RNA competition for dCas9 (Huang et al., 2021). We observe that modest overexpression of off-target scRNA has minimal effects on CRISPRa levels (Figure S15), consistent with recent modeling work suggesting favorable scaling for CRISPRa networks as compared with CRISPRi (Clamons and Murray, 2019). Taken together, these results suggest that the CRISPRa/i system could support the operation of programs containing up to 20 independent sc/sgRNAs with minimal impact to system performance in both CFS and *E. coli*. As CRIPSRa/i circuits become larger, it may be necessary to incorporate improvements from the larger CRISPR community with our approach to overcome potential limitations imposed by expression burden and gRNA competition (Huang et al., 2021; Schmidt et al., 2021)

In both natural and engineered systems RNA-based regulatory approaches provide a means for fast and metabolically efficient control of gene expression (Bobrovskyy and Vanderpool, 2013; Chappell et al., 2017; Stevens and Carothers, 2015; Takahashi et al., 2015; Westbrook et al., 2019). In multi-layer CRISPRa/i circuits, the speed of signal propagation is a tunable parameter depending on the relative expression levels of all components involved in both CFS and *E. coli*. Our analysis of relative production rates shows that guide RNA-mediated information propagation through internal layers of CRISPRa/i circuits can be fast (~30 min/layer) (Figure S14) compared with the time required for initial expression of functional CRISPRa components. Under saturating expression of dCas9, sgRNA titrations reveal an initial 40–50 min delay to the onset of CRISPRi, which could be attributed to maturation of dCas9 and formation of active CRISPR complexes (Figure 1E, right). Likewise, at high expression levels of dCas9, we observe small differences in the timing of gene expression across a wide range of scRNA expression levels (Figures 1D and S5, right). In CFS, CRISPRa-controlled production rates reach steady state with respect to constitutive expression over the course of several hours (Figure 1D, right). In contrast, CRISPR activation generated by cascades can experience minimal additional delays compared with CRISPRa in a single layer (Figure S14). For many applications in biocomputing and metabolic control, successful operation is determined not only by the fidelity but also the speed at which information is propagated through the regulatory network. CFS containing pre-expressed dCas9 and activator protein could accelerate the onset of CRISPRa/i regulation in these systems. Extrapolation of these CFS observations to inform the speed of propagation in *E. coli* is difficult because *E. coli* experience dilution due to cell division as well as dCas9 eviction due to DNA replication. While the cell-free experiments in this work were conducted as batch mode reactions, introduction of component turnover either through continuously diluted cell-free reactions (Dubuc et al., 2019; Karzbrun et al., 2014; Niederholtmeyer et al., 2013), or programmable degradation (Garamella et al., 2016) presents a bridge between cellular and cell-free settings. Future work to characterize the correspondence between tuning actions and the speed of signal propagation in cell-free systems with component turnover could provide a promising test bed to inform the predictive design of CRISPRa/i programs controlling gene expression timing in a cellular setting.

Given the previously demonstrated orthogonality of CRISPR-based regulation and the independence of CRISPRa/i nodes observed in this work, we find the CRISPRa/i system to be readily composable into larger motifs. CRISPRa/i circuits can be built by level-matching the response curves of different nodes, without complications arising from retroactivity and crosstalk. Indeed, upon construction of two orthogonal I1-FFLs in the same CFS reaction (Figure 3A), expression dynamics of the first I1-FFL were independent from both the presence and action of the second I1-FFL and nearly identical to expression dynamics observed in isolation. Such orthogonality enables design of circuits with deterministic functions based solely on proper implementation of network topologies. In CFS, we built circuits capable of generating distinct gene expression profiles determined by the specific network topologies (Figure 3A). We showed that expression dynamics are tunable through component expression levels within a given circuit topology when there is overlap between upstream and downstream circuit layers (Figures 2E and 3B). In *E. coli*, continuous dilution experiments revealed I1-FFL gene expression dynamics to be an almost perfect superposition of the dynamics of CRISPRa and an activation-repression cascade (Figure 6B). This composability is also captured by the relatively simple CFS CRISPRa/i model, which only specifies CRISPR complex

assembly and node-targeting reactions for each sc/sgRNA (Table S3). Paired with advancements in high-throughput component characterization in CFS and state-of-the-art modeling frameworks (Lehr et al., 2019; Moore et al., 2018; Poole et al., 2020), the CRISPRa/i system presents a route toward scalable computer-aided design and implementation of dynamic gene regulatory networks in CFS.

Overall, this work establishes a paradigm in which CRISPRa/i system components can be easily combined to form scalable, dynamic gene regulatory networks in CFS and *E. coli*. The CRISPRa/i system has proven capable of building layered operations and simultaneously executing multiple regulatory programs without compromising guideRNA-encoded expression dynamics. The dynamic gene expression profiles arising from CRISPRa/i regulation are composable, in that network expression dynamics can be understood as the aggregate of the constituent components in both CFS and *E. coli* (Figures 3B and 6B). These attributes allow rational design of CRISPRa/i circuits to tailor expression dynamics of multiple genes independently and simultaneously. We anticipate broad-ranging applications in engineered bacterial hosts, CFS, and the next generation of artificial cells. Specifically, we foresee applications in metabolic engineering, with feedforward motifs providing time-ordered enzyme expression, and tunable delays enabling phenotype switching in multi-phase reactions. For biosensing applications, the scalable and versatile nature of the CRISPRa/i system will allow combinatorial logical responses and complex input-output relationships to be specified, increasing the ease of connecting sensing to reporting stages. Finally, as synthetic biology efforts transition from repurposing natural systems to the bottom-up construction of fully artificial cells, the CRISPRa/i system could be a foundational technology capable of implementing the complex dynamic control of gene expression observed in nature, while remaining compact, robust, and engineerable.

STAR★METHODS

Detailed methods are provided in the online version of this paper and include the following:

- KEY RESOURCES TABLE
- RESOURCE AVAILABILITY
  - Lead contact
  - Materials availability
  - Data and code availability
- METHOD DETAILS
  - Plasmid design and preparation
  - Cell-free system preparation
  - Cell-free gene expression reaction
  - *E. coli* experiments
  - Constitutive CRISPRa experiments
  - aTc-inducible CRISPRa experiments
  - Continuous dilution *E. coli* experiments
  - CFS CRISPRa/i modeling
- QUANTIFICATION AND STATISTICAL ANALYSIS
  - Cell-free data analysis
  - *E. coli* data analysis
  - Statistics

SUPPLEMENTAL INFORMATION

Supplemental information can be found online at https://doi.org/10.1016/j.cels.2021.10.008.

ACKNOWLEDGMENTS

We thank members of the Carothers and Zalatan groups for advice, materials, and comments on the manuscript. This work was supported by US National Science Foundation (NSF) award CBET 1844152 (to J.M.C. and V.N.), NSF Award MCB 1817623 (to J.G.Z. and J.M.C.) and NSF Award EF-1935087 (to J.M.C.).

AUTHOR CONTRIBUTIONS

B.I.T., D.A.B., V.P.C., and J.M.C. designed the research; B.I.T., D.A.B., V.P.C., and A.K. performed experiments; B.I.T., C.K., and J.F. engineered components for CRISPRa; B.I.T., D.A.B., V.P.C., C.K., and A.K. analyzed the data. B.I.T., D.A.B., J.G.Z., and J.M.C. wrote the manuscript with input from all of the authors.

DECLARATION OF INTERESTS

J.F. is a founder of Wayfinder Biosciences, and J.G.Z. and J.M.C are members of the Wayfinder Biosciences scientific advisory board; all three are listed as co-inventors of RNA technologies that are the subjects of patent filings. The Noireaux laboratory receives research funds from Arbor Biosciences, a distributor of the myTXTL cell-free protein synthesis kit.

INCLUSION AND DIVERSITY

One or more of the authors of this paper self-identifies as an underrepresented ethnic minority in science.

Received: June 8, 2021
Revised: August 24, 2021
Accepted: October 26, 2021
Published: November 19, 2021

REFERENCES

Adamala, K.P., Martin-Alarcon, D.A., Guthrie-Honea, K.R., and Boyden, E.S. (2017). Engineering genetic circuit interactions within and between synthetic minimal cells. Nat. Chem. *9*, 431–439.

Adler, M., and Alon, U. (2018). Fold-change detection in biological systems. Curr. Opin. Syst. Biol. *8*, 81–89.

Adler, M., Szekely, P., Mayo, A., and Alon, U. (2017). Optimal regulatory circuit topologies for fold-change detection. Cell Syst. *4*, 171–181.e8.

Akaike, H. (1974). A new look at the statistical model identification. IEEE Trans. Automat Contr. *19*, 716–723.

Alon, U. (2007). Network motifs: theory and experimental approaches. Nat. Rev. Genet. *8*, 450–461.

Banerjee, D., Eng, T., Lau, A.K., Sasaki, Y., Wang, B., Chen, Y., Prahl, J.P., Singan, V.R., Herbert, R.A., Liu, Y., et al. (2020). Genome-scale metabolic rewiring improves titers rates and yields of the non-native product indigoidine at scale. Nat. Commun. *11*, 5385.

Bartoli, V., di Bernardo, M., and Gorochowski, T.E. (2020). Self-adaptive biosystems through tunable genetic parts and circuits. Curr. Opin. Syst. Biol. *24*, 78–85.

Bikard, D., Jiang, W., Samai, P., Hochschild, A., Zhang, F., and Marraffini, L.A. (2013). Programmable repression and activation of bacterial gene expression using an engineered CRISPR-Cas system. Nucleic Acids Res *41*, 7429–7437.

Bobrovskyy, M., and Vanderpool, C.K. (2013). Regulation of bacterial metabolism by small RNAs using diverse mechanisms. Annu. Rev. Genet. *47*, 209–232.

Brockman, I.M., and Prather, K.L.J. (2015). Dynamic metabolic engineering: new strategies for developing responsive cell factories. Biotechnol. J. *10*, 1360–1369.

Brophy, J.A.N., and Voigt, C.A. (2014). Principles of genetic circuit design. Nat. Methods *11*, 508–520.

Burnham, K.P., and Anderson, D.R. (2002). Model Selection and Multimodel Inference: A Practical Information-Theoretic Approach (Springer-Verlag).

Cavanaugh, J.E. (1997). Unifying the derivations for the Akaike and corrected Akaike information criteria. Stat. Probab. Lett. *33*, 201–208.

Chappell, J., Westbrook, A., Verosloff, M., and Lucks, J.B. (2017). Computational design of small transcription activating RNAs for versatile and dynamic gene regulation. Nat. Commun. *8*, 1051.

Choi, K., Medley, J.K., König, M., Stocking, K., Smith, L., Gu, S., and Sauro, H.M. (2018). Tellurium: An extensible python-based modeling environment for systems and synthetic biology. Biosystems *171*, 74–79.

Clamons, S., and Murray, R. (2019). Modeling predicts that CRISPR-based activators, unlike CRISPR-based repressors, scale well with increasing gRNA competition and dCas9 bottlenecking. bioRxiv https://www.biorxiv.org/content/10.1101/719278v2.

Dinh, C.V., and Prather, K.L. (2020). Layered and multi-input autonomous dynamic control strategies for metabolic engineering. Curr. Opin. Biotechnol. *65*, 156–162.

Dinh, C.V., and Prather, K.L.J. (2019). Development of an autonomous and bifunctional quorum-sensing circuit for metabolic flux control in engineered *Escherichia coli*. Proc. Natl. Acad. Sci. USA *116*, 25562–25568.

Dong, C., Fontana, J., Patel, A., Carothers, J.M., and Zalatan, J.G. (2018). Synthetic CRISPR-Cas gene activators for transcriptional reprogramming in bacteria. Nat. Commun. *9*, 2489.

Dubuc, E., Pieters, P.A., van der Linden, A.J., van Hest, J.C., Huck, W.T., and de Greef, T.F. (2019). Cell-free microcompartmentalised transcription–translation for the prototyping of synthetic communication networks. Curr. Opin. Biotechnol. *58*, 72–80.

Dudley, Q.M., Karim, A.S., and Jewett, M.C. (2015). Cell-free metabolic engineering: biomanufacturing beyond the cell. Biotechnol. J. *10*, 69–82.

English, M.A., Gayet, R.V., and Collins, J.J. (2021). Designing biological circuits: synthetic biology within the operon model and beyond. Annu. Rev. Biochem. *90*, 221–244.

Fontana, J., Dong, C., Ham, J.Y., Zalatan, J.G., and Carothers, J.M. (2018b). Regulated expression of sgRNAs tunes CRISPRi in E. coli. Biotechnol. J. *13*, e1800069.

Fontana, J., Dong, C., Kiattisewee, C., Chavali, V.P., Tickman, B.I., Carothers, J.M., and Zalatan, J.G. (2020). Effective CRISPRa-mediated control of gene expression in bacteria must overcome strict target site requirements. Nat. Commun. *11*, 1618.

Fontana, J., Voje, W.E., Zalatan, J.G., and Carothers, J.M. (2018a). Prospects for engineering dynamic CRISPR–Cas transcriptional circuits to improve bioproduction. J. Ind. Microbiol. Biotechnol. *45*, 481–490.

Gander, M.W., Vrana, J.D., Voje, W.E., Carothers, J.M., and Klavins, E. (2017). Digital logic circuits in yeast with CRISPR-dCas9 NOR gates. Nat. Commun. *8*, 15459.

Garamella, J., Marshall, R., Rustad, M., and Noireaux, V. (2016). The all E. coli TX-TL toolbox 2.0: a platform for cell-free synthetic biology. ACS Synth. Biol. *5*, 344–355.

Goentoro, L., Shoval, O., Kirschner, M.W., and Alon, U. (2009). The incoherent feedforward loop can provide fold-change detection in gene regulation. Mol. Cell *36*, 894–899.

Ho, H.I., Fang, J.R., Cheung, J., and Wang, H.H. (2020). Programmable CRISPR-Cas transcriptional activation in bacteria. Mol. Syst. Biol. *16*, e9427.

Huang, H.H., Bellato, M., Qian, Y., Cárdenas, P., Pasotti, L., Magni, P., and Del Vecchio, D. (2021). dCas9 regulator to neutralize competition in CRISPRi circuits. Nat. Commun. *12*, 1692.

Jeong, D., Klocke, M., Agarwal, S., Kim, J., Choi, S., Franco, E., and Kim, J. (2019). Cell-free synthetic biology platform for engineering synthetic biological circuits and systems. Methods Protoc. *2*, 39.

Kaplan, S., Bren, A., Dekel, E., and Alon, U. (2008). The incoherent feed-forward loop can generate non-monotonic input functions for genes. Mol. Syst. Biol. *4*, 203.

Karim, A.S., Dudley, Q.M., and Jewett, M.C. (2016). Cell-free synthetic systems for metabolic engineering and biosynthetic pathway prototyping. In Industrial Biotechnology (John Wiley & Sons), pp. 125–148.

Karzbrun, E., Tayar, A.M., Noireaux, V., and Bar-Ziv, R.H. (2014). Synthetic biology. Programmable on-chip DNA compartments as artificial cells. Science *345*, 829–832.

Kiattisewee, C., Dong, C., Fontana, J., Sugianto, W., Peralta-Yahya, P., Carothers, J.M., and Zalatan, J.G. (2021). Portable bacterial CRISPR transcriptional activation enables metabolic engineering in Pseudomonas putida. Metab. Eng. *66*, 283–295.

Landberg, J., Wright, N.R., Wulff, T., Herrgård, M.J., and Nielsen, A.T. (2020). CRISPR interference of nucleotide biosynthesis improves production of a single-domain antibody in Escherichia coli. Biotechnol. Bioeng. *117*, 3835–3848.

Lehr, F.X., Hanst, M., Vogel, M., Kremer, J., Göringer, H.U., Suess, B., and Koeppl, H. (2019). Cell-free prototyping of AND-logic gates based on heterogeneous RNA activators. ACS Synth. Biol. *8*, 2163–2173.

Liu, Y., Wan, X., and Wang, B. (2019). Engineered CRISPRa enables programmable eukaryote-like gene activation in bacteria. Nat. Commun. *10*, 3693.

Liu, Y., Zeng, Y., Liu, L., Zhuang, C., Fu, X., Huang, W., and Cai, Z. (2014). Synthesizing AND gate genetic circuits based on CRISPR-Cas9 for identification of bladder cancer cells. Nat. Commun. *5*, 5393.

Lucks, J.B., Qi, L., Whitaker, W.R., and Arkin, A.P. (2008). Toward scalable parts families for predictable design of biological circuits. Curr. Opin. Microbiol. *11*, 567–573.

Mangan, S., and Alon, U. (2003). Structure and function of the feed-forward loop network motif. Proc. Natl. Acad. Sci. USA *100*, 11980–11985.

Marshall, R., Maxwell, C.S., Collins, S.P., Jacobsen, T., Luo, M.L., Begemann, M.B., Gray, B.N., January, E., Singer, A., He, Y., et al. (2018). Rapid and scalable characterization of CRISPR technologies using an E. coli cell-free transcription-translation system. Mol. Cell *69*, 146–157.e3.

Marshall, R., and Noireaux, V. (2018). Synthetic biology with an all E. coli TXTL system: quantitative characterization of regulatory elements and gene circuits. In Synthetic Biology: Methods and Protocols, J.C. Braman, ed. (Springer), pp. 61–93.

McDaniel, R., and Weiss, R. (2005). Advances in synthetic biology: on the path from prototypes to applications. Curr. Opin. Biotechnol. *16*, 476–483.

Medley, J.K., Choi, K., König, M., Smith, L., Gu, S., Hellerstein, J., Sealfon, S.C., and Sauro, H.M. (2018). Tellurium notebooks—An environment for reproducible dynamical modeling in systems biology. PLOS Computational Biology *14*, e1006220.

Moore, S.J., MacDonald, J.T., Wienecke, S., Ishwarbhai, A., Tsipa, A., Aw, R., Kylilis, N., Bell, D.J., McClymont, D.W., Jensen, K., et al. (2018). Rapid acquisition and model-based analysis of cell-free transcription–translation reactions from nonmodel bacteria. Proc. Natl. Acad. Sci. USA *115*, E4340–E4349.

Niederholtmeyer, H., Stepanova, V., and Maerkl, S.J. (2013). Implementation of cell-free biological networks at steady state. Proc. Natl. Acad. Sci. USA *110*, 15985–15990.

Nielsen, A.A., and Voigt, C.A. (2014). Multi-input CRISPR/Cas genetic circuits that interface host regulatory networks. Mol. Syst. Biol. *10*, 763.

Nielsen, A.A., Der, B.S., Shin, J., Vaidyanathan, P., Paralanov, V., Strychalski, E.A., Ross, D., Densmore, D., and Voigt, C.A. (2016). Genetic circuit design automation. Science *352*, aac7341.

Poole, W., Pandey, A., Shur, A., Tuza, Z.A., and Murray, R.M. (2020). BioCRNpyler: compiling chemical reaction networks from biomolecular parts in diverse contexts. bioRxiv https://www.biorxiv.org/content/10.1101/2020.08.02.233478v2.full.

Qi, L.S., Larson, M.H., Gilbert, L.A., Doudna, J.A., Weissman, J.S., Arkin, A.P., and Lim, W.A. (2013). Repurposing CRISPR as an RNA-guided platform for sequence-specific control of gene expression. Cell *152*, 1173–1183.

Qian, Y., Huang, H.H., Jiménez, J.I., and Del Vecchio, D. (2017). Resource competition shapes the response of genetic circuits. ACS Synth. Biol. *6*, 1263–1272.

Reis, A.C., Halper, S.M., Vezeau, G.E., Cetnar, D.P., Hossain, A., Clauer, P.R., and Salis, H.M. (2019). Simultaneous repression of multiple bacterial genes using nonrepetitive extra-long sgRNA arrays. Nat. Biotechnol. *37*, 1294–1301.

Rosenfeld, N., and Alon, U. (2003). Response delays and the structure of transcription networks. J. Mol. Biol. *329*, 645–654.

Santos-Moreno, J., and Schaerli, Y. (2020). CRISPR-based gene expression control for synthetic gene circuits. Biochem. Soc. Trans. *48*, 1979–1993.

Santos-Moreno, J., Tasiudi, E., Stelling, J., and Schaerli, Y. (2020). Multistable and dynamic CRISPRi-based synthetic circuits. Nat. Commun. *11*, 2746.

Schmidt, M.J., Gupta, A., Bednarski, C., Gehrig-Giannini, S., Richter, F., Pitzler, C., Gamalinda, M., Galonska, C., Takeuchi, R., Wang, K., et al. (2021). Improved CRISPR genome editing using small highly active and specific engineered RNA-guided nucleases. Nat. Commun. *12*, 4219.

Shen-Orr, S.S., Milo, R., Mangan, S., and Alon, U. (2002). Network motifs in the transcriptional regulation network of Escherichia coli. Nat. Genet. *31*, 64–68.

Shin, J., and Noireaux, V. (2012). An E. coli cell-free expression toolbox: application to synthetic gene circuits and artificial cells. ACS Synth. Biol. *1*, 29–41.

Stevens, J.T., and Carothers, J.M. (2015). Designing RNA-based genetic control systems for efficient production from engineered metabolic pathways. ACS Synth. Biol. *4*, 107–115.

Sun, Z.Z., Hayes, C.A., Shin, J., Caschera, F., Murray, R.M., and Noireaux, V. (2013). Protocols for implementing an Escherichia coli based TX-TL cell-free expression system for synthetic biology. J. Vis. Exp. *79*, e50762.

Takahashi, M.K., Hayes, C.A., Chappell, J., Sun, Z.Z., Murray, R.M., Noireaux, V., and Lucks, J.B. (2015). Characterizing and prototyping genetic networks with cell-free transcription–translation reactions. Methods *86*, 60–72.

Tan, S.I., and Ng, I.S. (2021). CRISPRi-mediated NIMPLY logic gate for fine-tuning the whole-cell sensing toward simple urine glucose detection. ACS Synth. Biol. *10*, 412–421.

Thieffry, D., Huerta, A.M., Pérez-Rueda, E., and Collado-Vides, J. (1998). From specific gene regulation to genomic networks: a global analysis of transcriptional regulation in Escherichia coli. BioEssays *20*, 433–440.

Tian, J., Yang, G., Gu, Y., Sun, X., Lu, Y., and Jiang, W. (2020). Developing an endogenous quorum-sensing based CRISPRi circuit for autonomous and tunable dynamic regulation of multiple targets in Streptomyces. Nucleic Acids Res *48*, 8188–8202.

Tian, T., Kang, J.W., Kang, A., and Lee, T.S. (2019). Redirecting metabolic flux via combinatorial multiplex CRISPRi-mediated repression for isopentenol production in Escherichia coli. ACS Synth. Biol. *8*, 391–402.

Wan, X., Volpetti, F., Petrova, E., French, C., Maerkl, S.J., and Wang, B. (2019). Cascaded amplifying circuits enable ultrasensitive cellular sensors for toxic metals. Nat. Chem. Biol. *15*, 540–548.

Wang, Y.H., Wei, K.Y., and Smolke, C.D. (2013). Synthetic biology: advancing the design of diverse genetic systems. Annu. Rev. Chem. Biomol. Eng. *4*, 69–102.

Westbrook, A., Tang, X., Marshall, R., Maxwell, C.S., Chappell, J., Agrawal, D.K., Dunlop, M.J., Noireaux, V., Beisel, C.L., Lucks, J., and Franco, E. (2019). Distinct timescales of RNA regulators enable the construction of a genetic pulse generator. Biotechnol. Bioeng. *116*, 1139–1151.

Wu, F., Shim, J., Gong, T., and Tan, C. (2020a). Orthogonal tuning of gene expression noise using CRISPR–Cas. Nucleic Acids Res *48*, e76.

Wu, Y., Chen, T., Liu, Y., Tian, R., Lv, X., Li, J., Du, G., Chen, J., Ledesma-Amaro, R., and Liu, L. (2020b). Design of a programmable biosensor-CRISPRi genetic circuits for dynamic and autonomous dual-control of metabolic flux in Bacillus subtilis. Nucleic Acids Res *48*, 996–1009.

Xiang, Y., Dalchau, N., and Wang, B. (2018). Scaling up genetic circuit design for cellular computing: advances and prospects. Nat. Comput. *17*, 833–853.

Zalatan, J.G., Lee, M.E., Almeida, R., Gilbert, L.A., Whitehead, E.H., La Russa, M., Tsai, J.C., Weissman, J.S., Dueber, J.E., Qi, L.S., and Lim, W.A. (2015). Engineering complex synthetic transcriptional programs with CRISPR RNA scaffolds. Cell *160*, 339–350.

STAR★METHODS

KEY RESOURCES TABLE

REAGENT or RESOURCE	SOURCE	IDENTIFIER
Bacterial and virus strains		
NEB Turbo *E. coli*	New England BioLabs	#C2984I
MG1655 *E. coli*	ATCC	Cat# 700926
Chemicals, Peptides, and Recombinant Proteins		
Anhydrotetracycline (hydrochloride)	Cayman Chemical	10009542
Phusion DNA polymerase	New England BioLabs	M0530L
MOPS EZ rich defined media	Teknova	M2105
LB media	Teknova	L9135
Critical commercial assays		
PureLink PCR Purification Kit	Invitrogen	Cat# K310001
96-well V-bottom plate	Costar	Cat#3363
Deposited data		
Experimental data	https://github.com/carothersresearch/CRISPRai_Circuits_2021	https://doi.org/10.5281/zenodo.5555400
Experimental models: Organisms/strains		
MG1655 *E. coli*: F^-, lambda$^-$, rph-1	ATCC	Cat# 700926
Recombinant DNA		
See Table S4 for a list of plasmids	addgene	https://www.addgene.org/plasmids/articles/28222993/
Software and algorithms		
Python 3.7.6	https://www.python.org	
Data analysis	https://github.com/carothersresearch/CRISPRai_Circuits_2021	https://doi.org/10.5281/zenodo.5555400
Other		
Cell-Free Transcription/Translation *E. coli* lysate	Vincent Noireaux	Garamella et al., 2016

RESOURCE AVAILABILITY

Lead contact

Further information and requests for resources and reagents should be directed to and will be fulfilled by the Lead Contact, James M. Carothers (jcaroth@uw.edu)

Materials availability

Plasmids generated in this study have been deposited at Addgene (https://www.addgene.org/plasmids/articles/28222993/).

Data and code availability

- All CFS and *E. coli* data have been deposited at https://github.com/carothersresearch/CRISPRai_Circuits_2021 and are publicly available as of the date of publication. DOIs are listed in the key resources table.
- All models and scripts used in this work have been deposited at https://github.com/carothersresearch/CRISPRai_Circuits_2021 and are publicly available as of the date of publication. DOIs are listed in the key resources table.
- Any additional information required to reanalyze the data reported in this paper is available from the lead contact upon request.

METHOD DETAILS

Plasmid design and preparation

Plasmid design and sequencing analyses were performed using Benchling sequence designer. All PCR amplification of plasmids and fragments used Phusion DNA polymerase in GC buffer. Primers were synthesized by IDT and resuspended into nuclease-free water.

All PCR reactions were treated with DpnI for longer than 1 hour and purified using Qiagen gel extraction kits. Plasmid assembly was achieved using 5X In-Fusion HD mastermix (Takara). Assembled plasmids were transformed into chemically competent NEB Turbo *E. coli* and plated onto LB-agar plates with either 100 μg/mL carbenicillin or 25 μg/mL chloramphenicol and grown overnight ~16 hours at 37 °C. Single colonies were picked from plates and grown overnight in LB shaking at 37 °C with appropriate concentrations of relevant antibiotics. Plasmids were isolated from subcultures using a DNA miniprep kit (QIAprep Spin Miniprep Kit) and Sanger sequenced (Genewiz inc.) to identify correctly assembled plasmids. Plasmids intended for use in CFS were grown in culture volumes ~20 mL to ensure adequate yields for multiple cell-free reactions. Plasmids intended for cell-free expression were further purified using a PCR purification kit (Invitrogen PureLink, Cat. K310001), and were eluted into nuclease-free water. Plasmid concentrations were quantified via spectrophotometry (Nanodrop 2000c, Cat. ND-2000C).

Cell-free system preparation

The cell-free system was prepared according to previously published procedures (Garamella et al., 2016; Sun et al., 2013). The cell-free system used for an experiment was thawed on ice and pooled into a 1.5 ml eppendorf tube, vortexed, and spun-down using a mini benchtop centrifuge to ensure homogeneity across samples.

Cell-free gene expression reaction

Cell-free gene expression reactions were assembled on ice from the CFS and purified DNA. A master mix with common plasmids across reactions was prepared, and 1.5 μL per reaction allocated into PCR tubes. Plasmids which were varied across reactions were added in the remaining 1 μL. The CFS was pipette mixed and added to each PCR tube in 7.5 μL for a final volume of 10 μL. PCR tubes were vortexed, spun-down using a mini benchtop centrifuge, and placed on ice. Triplicates of 2.5 μL for each reaction were pipetted into individual wells of a 96-well V-bottom plate (Costar, Cat. 3363). The plate was sealed (Costar, Cat. 3080) and analyzed on a BioTek Synergy HTX plate reader at 29 °C. sfGFP fluorescence (ex. 485 nm, em. 528 nm) and mRFP1 fluorescence (ex. 540 nm, em. 600 nm) of cell-free reactions were measured every 10 min from the bottom of the plate. All reactions were run in batch mode.

E. coli experiments

Circuits were assembled in *E. coli* through transformation of plasmid pairs. In all *E. coli* experiments CRISPRa system components (dCas9, MCP-SoxS, input sc/sgRNAs) are located on a p15A ori (copy number ~10) plasmid while sc/sgRNAs forming the second layer of a circuit were cloned into the reporter plasmid with a pSC101** ori (copy number ~5) due to the size difference between vectors. The p15A plasmid used in constitutive CRISPRa experiments was pCK085. aTc-inducible CRISPRa experiments use pJF182 in which pTet controls expression of TetR and MCP-SoxS. Plate reader measurements were conducted using a BioTek Synergy HTX with a black flat bottom plate (Ref# 3631) using 100 μL of culture.

Constitutive CRISPRa experiments

Endpoint CRISPRa experiments are conducted using constitutive expression of all CRISPRa components (pCK085). Circuits were assembled by transformation of CRISPRa and reporter plasmids into chemically competent MG1655 E. coli. Transformed E. coli were outgrown for 1 hour shaking at 37 °C and plated onto LB-agar with carbenicillin and chloramphenicol. Plates were grown overnight at 37 °C. Experiments were conducted by picking three individual colonies into 400 μL Teknova EZ-RDM with 0.2% glucose and appropriate antibiotics in 96 well plates (round 2 ml), covering with breathable membrane (Breathe Easier cat# Z763624) and shaking overnight at 37 °C at 1200 RPM on a Heidolph titramax 1000.

aTc-inducible CRISPRa experiments

For inducible CRISPRa experiments expression of activator protein MCP-SoxS was controlled by pTet. Upon addition of aTc (anhydrotetracycline) to media, pTet becomes de-repressed which enables titratable expression of MCP-SoxS activator. As above, circuits are assembled by transformation of CRISPRa and reporter plasmids into chemically competent MG1655 *E. coli*. Transformed *E. coli* were outgrown for 1 hour shaking at 37 °C and plated onto LB-agar with carbenicillin and chloramphenicol. Plates were grown overnight at 37 °C. Experiments were conducted by picking three individual colonies into 400 uL EZ-RDM with 0.2% glucose and appropriate antibiotics in 96 well plates (2ml). Cultures are covered with breathable membrane and left shaking overnight at 37 °C at 1200 RPM on a Heidolph titramax 1000. Overnight cultures are subsequently diluted 1:40 into a fresh plate of EZ-RDM and incubated at 37 °C shaking at 1200 RPM. Before exiting exponential phase (~3 hours) cultures are diluted 1:40 into a fresh plate of EZ-RDM and supplemented with appropriate concentrations of aTc. These cultures are again covered with a breathable membrane, incubated in the dark at 37 °C shaking at 1200 RPM, and grown overnight ~18 hours. Measurements are conducted in Costar 96 well black flat bottom plates in 100 uL culture volume.

Continuous dilution *E. coli* experiments

Strains used in continuous dilution experiments were constructed as above through double transformation with appropriate selection on plates. For CRISPRa and I1-FFL experiments MG1655 was used while for CRISPRa/i cascades, MG1655 with an integrated reporter (J23119-RFP) was used (Fontana et al., 2018b). Throughout the experiment all steps including liquid handling were conducted at 37 °C. Individual colonies were picked and grown overnight in 500 μL of LB with appropriate antibiotics shaking at

1200 RPM in a 96 well deep well plate. In the morning cultures were diluted 1:50 into RZ-RDM with 0.2% glucose and grown as before for one hour at a total volume of 300 μl. At one hour, 100 μL of culture was removed and measured while 100 μL fresh pre-warmed media was added to each culture. This process was repeated every 20 minutes until OD_{600} stabilized, usually within ~1-2 hours. Once ODs stabilized, aTc inducer was added to cultures to a final concentration of 50 nM. Every 20 minutes for the remainder of the experiment (~8 hours), 100 μL culture was removed and measured, while the culture was resupplied with 100 μL pre-warmed inducing media.

CFS CRISPRa/i modeling

The CFS CRISPRa/i model was defined as a series of first order chemical reactions for protein and guide RNA production, CRISPR complex assembly, and DNA targeting. The model was implemented using the text-based model definition language Antimony for Python 3.7 (Table S3). Here we also present the underlying system of differential equations governing the model.

The general CRISPRa/i model is based on the different transcriptional states a CRISPRa/i node can take. At the DNA level, each node D_i can either be unregulated, activated by CRISPRa (D_i^A), or repressed by CIRSPRi (D_i^R). We differentiate between two different repression states based on whether CRISPRa is also bound. The ODEs defining the change in concentration over time between node states are therefore:

$$\frac{dD_i}{dt} = -k_{on}\left[C_i^A \cdot D_i + C_i^R \cdot D_i\right]$$

$$\frac{dD_i^A}{dt} = k_{on}\left[C_i^A \cdot D_i - C_i^R \cdot D_i^A\right]$$

$$\frac{dD_i^R}{dt} = \frac{dD_i^{R_1}}{dt} + \frac{dD_i^{R_2}}{dt} = k_{on}\left[C_i^R \cdot D_i - C_i^A \cdot D_i^{R_1}\right] + k_{on}\left[C_i^R \cdot D_i^A + C_i^A \cdot D_i^{R_1}\right]$$
$$= k_{on} \cdot C_i^R\left[D_i + D_i^A\right]$$

Where C_i^A and C_i^R represent the concentration of free CRISPRa and CRIPSRi complexes targeting node i, respectively, and k_{on} is the rate of association to the DNA, assuming a one-step irreversible reaction.

The concentration of free CRISPR complexes is determined by the association rate of the different components (dCas9 C, scRNA G_i^A, and MCP-SoxS S for CRIPSRa; dCas9 C and sgRNA G_i^R for CRISPRi) as well as the rate at which they bind to the respective targets, namely:

$$\frac{dC_i^A}{dt} = k_A \cdot C \cdot G_i^A \cdot S - k_{on} \cdot C_i^A\left[D_i + D_i^{R_1}\right] = K_A - k_{on} \cdot C_i^A\left[D_i + D_i^{R_1}\right]$$

$$\frac{dC_i^R}{dt} = k_R \cdot C \cdot G_i^R - k_{on} \cdot C_i^R\left[D_i + D_i^A\right] = K_R - k_{on} \cdot C_i^R\left[D_i + D_i^A\right]$$

The concentration of the different protein and RNA species is based on their expression and interactions with other components. For simplicity, here protein transcription and translation are lumped.

$$\frac{dP_i^{off}}{dt} = k_T \cdot D_i + k_{TA} \cdot D_i^A - k_M \cdot P_i^{off} - \Gamma, \Gamma = \begin{cases} K_A + K_R, \text{if } P_i = C \\ K_A, \text{if } P_i \end{cases}$$
$$= S \quad \varnothing, \quad \text{otherwise}$$
$$\frac{dP_i}{dt} = k_M \cdot P_i^{off};$$

$$\frac{dR_i}{dt} = k_T \cdot D_i + k_{TA} \cdot D_i^A - k_D \cdot R_i - Y, Y = \begin{cases} K_A, & \text{if } R_i = G_i^A K_R, \\ & \text{if } R_i = G_i^R \end{cases}$$

Parameters were generated from log-uniform distributions spanning 4 orders of magnitude based around literature values or best estimates. Models with different parameters were evaluated using Tellurium (Choi et al., 2018; Medley et al., 2018), and the model outputs were processed in the same manner as the experimental data. The processed outputs were then fit to scaled RFP production rates of experimental data by minimizing the cumulative point-wise squared error using the Nelder-Mead simplex algorithm.

QUANTIFICATION AND STATISTICAL ANALYSIS

Cell-free data analysis

Production rate

Throughout this work, we define production rate as:

$$\dot{B}^{\alpha}(t) = \frac{dB^{\alpha}}{dt} = \frac{B^{\alpha}(t+30) - B^{\alpha}(t)}{30}$$

where:

B is the measured quantity: RFP or GFP

α specifies the circuit topology and relevant plasmid concentrations

Relative production rates

Relative production rates of CRISPRa mediated outputs were calculated as the ratio of CRISPRa mediated production rates divided by unregulated production rates. For CRISPRa the contribution due to unregulated basal expression was subtracted from measured output levels due to CRISPRa. This was done to isolate the timing of CRISPRa mediated gene expression from the comparatively early contribution of basal expression, and to allow observation of CRISPRa mediated gene expression dynamics under conditions where basal expression of reporter constructs dominates. Throughout this work, relative production rates are abbreviated as Rel. RFP Prod. Rate, or Rel. GFP Prod. Rate, and are calculated as:

$$\dot{B}^{\alpha}_{\Gamma}(t) = \frac{\dot{B}^{\alpha}(t) - \dot{B}^{\Gamma}(t)}{\dot{B}^{\Gamma}(t)}$$

where:

α is a specific CRISPRa/i circuit

Γ is constitutive expression

For CRISPRi mediated relative production rates there is no subtraction of basal expression and relative production rates are provided as:

$$\dot{B}^{\alpha}_{\Gamma}(t) = \frac{\dot{B}^{\alpha}(t)}{\dot{B}^{\Gamma}(t)}$$

Fold change in cascade output

In Figure 2B, fold change in cascade output was calculated as the ratio of RFP values generated by the CRISPRa cascade compared to CRISPRa in a single layer with the same concentration of scRNA expressing plasmid Y.

$$FC^{\alpha}_{\beta}(y) = \frac{\frac{B^{\alpha}(t=t_{max})}{B^{\Gamma}(t=t_{max})}}{\frac{B^{\beta}(t=t_{max})}{B^{\Gamma}(t=t_{max})}} = \frac{B^{\alpha}(t=t_{max})}{B^{\beta}(t=t_{max})}$$

where:

B is measured RFP

α is CRISPRa cascade, with y nM scRNA Y

β is CRISPRa, with y nM scRNA Y

t_{max} is the endpoint time of the cell free reaction

Predicted fold change in cascade output

Predicted fold change in cascade output plotted in Figure 2B was generated using the fits to scRNA titration curves provided in 2A (red line). Predicted fold changes provided by CRISPRa at a given concentration of scRNA expressing plasmid y are denoted: $\widehat{FC}^{\alpha}_{\Gamma}(y)$. In this experiment, CRISPRa in the first layer of the cascade (2A, left) generated by x nM of scRNA at node X is expected to direct a 24-fold increase in transcription from the target. Thus, for a given concentration of scRNA expressing plasmid y at node Y in the second layer of the cascade, predicted fold change in cascade output is calculated as the ratio of fold changes predicted by the fit in the right panel of 2A at a scRNA concentration of 24y, and 1y.

$$\widehat{FC}^{\alpha}_{\beta}(y) = \frac{\widehat{FC}^{\alpha}_{\Gamma}(24y)}{FC^{\alpha}_{\Gamma}(y)}$$

where:

is CRISPRa cascade, with y nM scRNA Y

is CRISPRa, with y nM scRNA Y

Normalized Z output

In Figures 2C and 2D normalized Z output is defined as the percent expression provided by CRISPRi or a CRISPRa/i cascade compared to an unregulated, constitutive expression control.

$$nB_I^{\alpha}(y) = 100 \cdot \frac{B^{\alpha}(t = t_{max})}{B^{I}(t = t_{max})}$$

where:

B is measured RFP

α is CRISPRi or a CRISPRa/i cascade with y nM sgRNA plasmid at node Y

Scaled relative production rates

In Figure 2E relative production rates were scaled by the observed production rate of the reaction at 40 mins to place curves on a common scale before the maturation of dCas9 and the onset of CRISPRa/i control.

$$s\dot{B}_I^{\alpha}(t) = \frac{\dot{B}_I^{\alpha}(t)}{\dot{B}_I^{\alpha}(t = 40)}$$

where:

$\dot{B}_I^{\alpha}$ is relative RFP production rate

α is CRISPRi or CRISPRa/i cascade with y nM sgRNA plasmid at node Y

Time to 50% repression

Time to 50% repression in Figures 2F and S4 was defined as the time at which relative production rates due to CRISPRa/i control first reached 50% of the initial 50 min value i.e., before maturation of dCas9 and the onset of CRISPRi.

$$t = t_{50\%} when \frac{\dot{B}_I^{\alpha}(t)}{\dot{B}_I^{\alpha}(t = 50)} \geq .5$$

where:

$\dot{B}_I^{\alpha}$ is relative RFP production rate

α is CRISPRi, or CRISPRa/i cascade with y nM sgRNA plasmid at node Y

Normalized relative RFP production rates

In Figure 3A relative RFP production rates are scaled by their respective endpoints to place curves on a common scale:

$$n\dot{B}_I^{\alpha}(t) = \frac{\dot{B}_I^{\alpha}(t)}{B^{\alpha}(t = t_{max})}$$

where:

B is measured RFP

$\dot{B}_I^{\alpha}$ is relative RFP production rate

α is CRISPRa, CRISPRa+i, or an I1-FFL

Scaled RFP production rate

In Figure 3B RFP production rates were scaled by their respective maxima, placing both curves on a common scale, allowing comparison of time dynamics.

$$s\dot{B}^{\alpha}(t) = \frac{\dot{B}^{\alpha}(t)}{max(\dot{B}^{\alpha}(t))}$$

where:

$\dot{B}(t)$ is RFP production rate

α is an I1-FFL with y =.1 nM or y = 1 nM sgRNA plasmid at node Y

Percent signal propagated by CRISPRa cascade

The percent signal propagated by the CRISPRa cascade in CFS was calculated as the fold change in cascade output ± input divided by the fold change provided by CRISPRa in the input layer.

$$SP(y) = 100 \cdot \frac{FC_{\beta_1}^{\alpha_1}(y)}{FC_I^{\beta_2}(y)}$$

where:

α_1 is CRISPRa cascade with y nM of scRNA at node Y

β_1 is CRISPRa with y nM of scRNA at node Y

β_2 is CRISPRa with x nM of scRNA at node X

Time to 2x activation

Time to 2-fold activation was defined as the time at which relative production rates are expected to first exceed 1, i.e., when CRISPRa mediated production rates first achieve twice that of unregulated expression. Time to 2-fold activation was calculated as the mean ± standard deviation from linear fits to relative RFP production rates for three technical replicates. Linear fits were calculated over a 1 hour interval between 80 and 160 mins corresponding to the initial linear increase in relative RFP production rates provided by CRISPRa.

$$t = t_{2x} when \dot{B}_{\Gamma}^{\alpha}(t) \geq 1.0$$

where:

$\dot{B}(t)$ is relative RFP production rate

α is CRISPRa with x nM scRNA at node X

Time to half maximal expression

In Figure S5B, time to half maximal expression was calculated differently for CRISPRa and CRISPRi. For CRISPRa the contribution due to unregulated basal expression was subtracted from measured RFP levels due to CRISPRa. This was done to isolate the timing of CRISPRa mediated gene expression from the comparatively early contribution of leak, and to allow observation of CRISPRa mediated gene expression dynamics under conditions where basal expression of reporter constructs dominates. The time to half max is denoted as $t_{1/2}$.

For CRISPRa this was defined as the first time point at which

$$t = t_{\frac{1}{2}} when \frac{B^{\alpha}(t) - B^{\Gamma}(t)}{B^{\alpha}(t = t_{max}) - B^{\Gamma}(t = t_{max})} \geq .5$$

where:

B is measured RFP

α is CRISPRa with x nM scRNA at node X

For CRISPRi there was no subtraction of basal expression thus time to half maximal expression for CRISPRi is given by the first time point at which

$$t = t_{\frac{1}{2}} when \frac{B^{\alpha}(t)}{B^{\alpha}(t = t_{max})} \geq .5$$

where:

B is measured RFP

α is CRISPRi with x nM scRNA at node X

Relative fold change

In Figure S12, the gene expression dynamics of CRISPRa and a CRISPRa cascade are compared to visualize the speed of signal propagation in multi-layer CRISPR circuits. For these data, fold change is a function of time:

$$rFC_{\Gamma}^{\alpha}(t, y) = \frac{FC_{\Gamma}^{\alpha}(t, y)}{FC_{\Gamma}^{\alpha}(t = t_{max}, y)}$$

where:

B is measured RFP

α is CRISPRa or CRISPRa cascade with y nM scRNA plasmid at node Y

y is the concentration of scRNA expressing plasmid in the final layer of the circuit

Normalized fluorescence

In Figure S7, RFP and GFP fluorescence were normalized by the response range for each fluorescent protein to lie on a common scale between 0 and 1.

$$nB = \frac{B\ (t = t_{max}) - min(B\ (t = t_{max}))}{max(B\ (t = t_{max})) - min(B\ (t = t_{max}))}$$

where:

B is a vector containing average RFP or GFP fluorescence for all tested conditions (CRISPRa, CRISPRa+i, I1-FFL, orthogonal I1-FFLs)

Number of possible network topologies

The number of possible network topologies presented in Figure S1 was calculated as:

$$T(M, N) = (M + 1) \cdot (N \cdot (N - 1))$$

where:

M is the number of modes of regulation

M = 1 for CRISPRi alone

M = 2 for both CRISPRa and CRISPRi together

N is the number of nodes in the network

***E. coli* data analysis**

Throughout this work all measured RFP levels in *E. coli* were normalized by measured OD_{600}. Data are plotted as the mean RFP/OD_{600} ± standard deviation of three biological replicates with appropriate propagation of uncertainties.

Span

In Figure 5C span was calculated in percent as the range of RFP expression values provided by CRISPRa/i cascades (0, 200nM aTc) divided by RFP expression levels obtained in the presence of off-target sgRNA.

$$S = \frac{B^{\alpha_1} - B^{\alpha_2}}{B^{\beta_1}}$$

where:

B is RFP/OD_{600} measured at endpoint

α_1 is CRISPRa/i cascade with 0 nM aTc induction

α_2 is CRISPRa/i cascade with 200 nM aTc induction

β_1 is CRISPRa/I cascade with off target sgRNA

Output dynamic range

Output dynamic range was calculated as the ratio of measured CRISPRa/i cascade RFP outputs at 0nM aTc and 200nM aTc. The inverse quantity was used for I1-FFL output dynamic range.

$$O - DR = \frac{B^{\alpha_1}}{B^{\alpha_2}}$$

where:

B is RFP/OD_{600} measured at endpoint

α_1 is CRISPRa/i cascade with 0 nM aTc induction

α_2 is CRISPRa/i cascade with 200 nM aTc induction

Relative RFP/OD_{600}

Relative RFP/OD_{600} presented in Figure 6B was calculated from raw RFP/OD_{600} data by subtraction of the minimum observed RFP/OD_{600} value post induction, and scaling outputs by their maximum observed values to place all curves on a scale between zero and one.

$$rB\ (t) = \frac{B\ (t) - min(B\ (t>t_0))}{max(B\ (t>t_0))}$$

where:

B is RFP/OD_{600} measured at endpoint

α is CRISPRa, CRISPRa/i cascade, or I1-FFl with 50 nM aTc induction

t_0 is the time at which aTc is added to the culture

Leak

In Figure S10 leak was calculated as the percent reduction of measured CRISPRa RFP levels at 200nM aTc induction, due to unactivated sgRNA expression.

$$L = 100 \cdot \frac{B - B^{\beta}}{B}$$

where:

B is RFP/OD600 measured at endpoint

α is CRISPRa at 200 nM aTc

β is CRISPRa+i at 200 nM aTc

Output Range Compression

Output range compression was defined as the output range of a CRISPRa/i circuit divided by the accessible output range. Here, output range of a CRISPRa/i cascade was defined as:

$$OR = B^{\alpha_1} - B^{\alpha_2}$$

While output range of CRISPRa was defined as:

$$OR = B^{\alpha_2} - B^{\alpha_1}$$

In a CRISPRa/i cascade, the accessible output range was calculated as the measured fluorescence provided by the CRISPRa/i cascade with an off target sgRNA

$$A = B^{\beta_1}$$

For I1-FFLs, the accessible output range was defined as the output range of the corresponding circuit with an off-target sgRNA, at 200 nM aTc and 0 nM aTc

$$A = B^{\beta_2} - B^{\beta_1}$$

While for CRISPRa+i, the accessible output range was defined as the output range with an off-target scRNA directing CRISPRa to activate sgRNA expression, at 200 nM aTc and 0 nM aTc

$$A = B^{\beta_2} - B^{\beta_1}$$

Thus, output range compression of CRISPRa/i cascades was defined in percent as:

$$ORC = 100 \cdot \left(1 - \frac{OR}{A}\right) = 100 \cdot \left(1 - \frac{B^{\alpha_1} - B^{\alpha_2}}{B^{\beta_1}}\right)$$

While output range compression of CRISPRa+I was defined as:

$$ORC = 100 \cdot \left(1 - \frac{OR}{A}\right) = 100 \cdot \left(1 - \frac{B^{\alpha_2} - B^{\alpha_1}}{B^{\beta_2} - B^{\beta_1}}\right)$$

where:

B is RFP/OD_{600} measured at endpoint
α_1 is CRISPRa+i, at 0 nM aTc
α_2 is CRISPRa+i, at 200 nM aTc
β_1 is CRISPRa+i, with off-target sgRNA at 0 nM aTc
β_2 is CRISPRa+i, with off-target sgRNA at 200 nM aTc

Percent CRISPRa induction

Percent CRISPRa induction presented in Figure S11 was calculated by dividing measured RFP values obtained from CRISPRa by the measured RFP value provided by CRISPRa at maximal, saturating levels of aTc induction (200nM).

$$\%I(x) = 100 \cdot \frac{B^{\alpha_1}}{B^{\alpha_2}}$$

where:

B is RFP/OD_{600} measured at endpoint
α_1 is CRISPRa at x nM aTc
α_2 is CRISPRa at 200 nM aTc

Statistics

Statistical significance was calculated using two-tailed unpaired Welch's t tests. When comparing two different models (Figures 6A and S13), statistical significance was assessed by calculating the relative likelihood (RL) between a logarithmic model and a linear model, based on the Akaike Information Criterion with small sample correction for each model (Akaike, 1974; Burnham and Anderson, 2002; Cavanaugh, 1997):

$$RL = exp\left(\frac{AIC_c(M_1) - AIC_c(M_2)}{2}\right)$$

$$AIC_c = 2 \cdot k + n \cdot log\left(\frac{\sum Res^2}{2}\right) + \frac{2 \cdot k \cdot (k+1)}{n - k - 1}$$

where n denotes the sample size, k denotes the number of parameters, Res the residuals, and M_1 and M_2 correspond to the linear and logarithmic models, respectively. Here the use of the AICc provides a second order estimation of information loss for each model. In addition to goodness of fit, the AICc takes into account the underlying model complexity and the size of the data set to penalize overfitting. For a given dataset, the model which minimizes the AICc can be said to minimize information loss. Within this paradigm, the relative likelihood is interpreted as the probability that M_2 minimizes information loss as compared to M_1.